


## Article

# Rule-Based Operation Mode Control Strategy for the Energy Management of a Fuel Cell Electric Vehicle

Jokin Uralde , Oscar Barambones \*, Asier del Rio , Isidro Calvo  and Eneko Artetxe 

Department of Systems Engineering and Automatic Control, Faculty of Engineering of Vitoria-Gasteiz, University of the Basque Country (UPV/EHU), 01006 Vitoria-Gasteiz, Spain; jokin.uralde@ehu.eus (J.U.); asier.delrio@ehu.eus (A.d.R.); isidro.calvo@ehu.eus (I.C.); eneko.artetxe@ehu.eus (E.A.)

\* Correspondence: oscar.barambones@ehu.eus

**Abstract:** Hydrogen, due to its high energy density, stands out as an energy storage method for the car industry in order to reduce the impact of the automotive sector on air pollution and global warming. The fuel cell electric vehicle (FCEV) emerges as a modification of the electric car by adding a proton exchange membrane fuel cell (PEMFC) to the battery pack and electric motor, that is capable of converting hydrogen into electric energy. In order to control the energy flow of so many elements, an optimal energy management system (EMS) is needed, where rule-based strategies represent the smallest computational burden and are the most widely used in the industry. In this work, a rule-based operation mode control strategy for the EMS of an FCEV validated by different driving cycles and several tests at the strategic points of the battery state of charge (SOC) is proposed. The results obtained in the new European driving cycle (NEDC) show the 12 kW battery variation of 2% and a hydrogen consumption of 1.2 kg/100 km compared to the variation of 1.42% and a consumption of 1.08 kg/100 km obtained in the worldwide harmonized light-duty test cycle (WLTC). Moreover, battery tests have demonstrated the optimal performance of the proposed EMS strategy.

**Keywords:** hydrogen car; fuel cell; energy management; rule-based control



**Citation:** Uralde, J.; Barambones, O.; del Rio, A.; Calvo, I.; Artetxe, E. Rule-Based Operation Mode Control Strategy for the Energy Management of a Fuel Cell Electric Vehicle. *Batteries* **2024**, *10*, 214. <https://doi.org/10.3390/batteries10060214>

Academic Editor: Chunwen Sun

Received: 10 May 2024

Revised: 6 June 2024

Accepted: 13 June 2024

Published: 19 June 2024



**Copyright:** © 2024 by the authors. Licensee MDPI, Basel, Switzerland. This article is an open access article distributed under the terms and conditions of the Creative Commons Attribution (CC BY) license (<https://creativecommons.org/licenses/by/4.0/>).

## 1. Introduction

Fossil fuels have been responsible for meeting the world's growing energy needs in the industrial and transport sectors, in the absence of the electrification of these sectors. In certain industries, this is still an impossible task, but in the transport and automotive sectors, where greenhouse gas emissions continue to rise and, major advances are possible [1,2]. The high-energy density of petroleum-based fuels is indeed crucial for enhancing the on-board storage capacity and extending the vehicle range. They are also cheap to manufacture, easy to handle, and quick to refill [3]. However, it is already known that fossil fuels are an unsustainable source and negatively affect the environment due to the emission of greenhouse gases (GHGs). In fact, the transport sector represents the 16.2% of all GHGs, of which road transport alone is 11.9% out of the 16.2% [4].

For this reason, in recent years, and mainly in the most developed countries, carbon neutral and related policies have been implemented [5]. This translates in the great growth of electricity as a source of energy for automobiles, namely the electric vehicle (EV). In fact, electric vehicles work through a portable energy storage system which tackles the issue of the unstable and intermittent energy generation of the renewable energy sources [6]. Furthermore, the European Parliament, agreed in the amendment that, by 2035, only cars powered by electric or hydrogen batteries will be available for purchase in EU countries [7]. The emissions cut for combustion vehicles is set at 37% now and 100% in 13 years. This means a ban on the manufacture and sale of diesel, petrol, and hybrid cars from 2035.

The EVs can work alongside batteries only (BEV), with an internal combustion engine (ICE) as Hybrid Electric Vehicle (HEV) in the case of hybrid electric vehicles (HEVs), or with

a fuel cell stack in the case of fuel cell electric vehicle (FCEVs) [8]. FCEVs emerge as a viable alternative aiming to bridge the gap between electric and traditional vehicles by harnessing the benefits of both. Despite the high efficiency of BEVs in converting grid energy into traction force and their capability to recuperate energy via regenerative braking during operation, a significant limitation stems from their typically restricted range, attributable to the size and cost of the necessary batteries to fulfil vehicle power and energy requirements. Additionally, the recharging process for battery systems often involves lengthy periods, contrasting sharply with the mere minutes needed to refuel a conventional ICE vehicle [9]. The role of hydrogen in automotive marking and the relevance of hydrogen cars is reflected in the increasing number of publications and references on FCEVs as described in [10]. Also, different car brands have already launched FCEVs such as the Hyundai Nexu (2018) or the Toyota Mirai (2021).

FCEVs use pure hydrogen stored in tanks as an energy source. This hydrogen is then used to produce electricity and power the electric motor as well as the battery pack. This process is performed by a proton exchange membrane fuel cell (PEMFC), an energy conversion device that uses a reverse electrolysis effect to provide electrical power. Thus, the environmental impact of the FECVs is minimal since the only tailpipe emission is water. However, it is important to consider the entire hydrogen production process alongside this. For the FCEV to be a truly zero emission vehicle, the hydrogen must be a so-called green hydrogen, obtained from the electrolysis of water and using renewable energy sources to power the process [11].

In a FECV, a fuel cell works alongside a battery or/and a super-capacitor, in order to provide the demanded power at any given moment and to harness the regenerative capacity of the electric motor. Thus, a correct energy management is needed to make an optimal use of each power source. This translates in the great amount of papers dedicated to discuss this task.

In [12], Oladosu et al. categorized energy management system (EMS) strategies based on rule-based techniques, optimization-based control, and artificial intelligence adaptive control systems. Rule-based control (RBC) has been widely used due to its easy logic and implementation although it is not very scalable. Precise design requirements may be needed to accommodate the complexities of the control strategy which is generally not feasible. Additionally, RBC shows another limitation in relation to the learning ability which makes impossible an update of the system impossible. It also shows a difficulty in managing control challenges that are not predefined at the design stage. Despite the disadvantages, RBC strategies show low computational cost, easy implementation, good real-time performance, and no need for information about driving conditions. Thus, the RBC is the most common strategy in the real hydrogen car industry, as exemplified the aforementioned Toyota Mirai and Hyundai Nexu [13].

RBC has been widely used in energy management tasks in different systems. In [14], for example, a rule-based strategy is used to control a multi-source grid to power an EV charging station and manage to minimize the power imported from the utility grid and maximize the power share from the renewable or stored energy consumption. In [15], on the other hand, a RBC-based global supervisory unit is designed for the electric energy management of an electric aircraft when eliminating the 5 min overload capability of the generator, and achieving that, any overload is cleared within 5 s. Inside FCEVs, a study of the multi-objective optimization problem with a rule-based control strategy was made in [16], achieving a hydrogen consumption of about 6–9 kg/100 km. Moreover, as proposed in [17], rule-based EMS could be hybridized with another control strategy such as artificial intelligence-based ones trying to compensate for the weakness of each.

Inside optimization-based control, online and offline optimization methods are differentiated. This type of control is introduced in response to the need for scalability, real-time local and global updating, and the flexibility to reduce the operational and maintenance cost which the RBC lacks. In online or real-time methods the equivalent consumption minimization strategy (ECMS) have been widely used as in [18], where an ECMS is used

for EMS in an autonomous FCEV. In the ECMS, the electrical consumption of the battery initially undergoes conversion into equivalent hydrogen consumption initially, followed by the minimization of the sum comprising the equivalent hydrogen consumption and the hydrogen consumption from the fuel cell. In [19], on the other hand, a sequential quadratic Programming (SQP) algorithm is added alongside an ECMS in order to reduce the hydrogen consumption while maintaining the PEMFC in the maximum efficiency region. The proposed ECMS showed an improvement of 12% in the hydrogen consumption while achieving a higher average efficiency of the FC over a conventional ECMS.

Model predictive control (MPC) is also among the real-time methods and has also been also studied. In [20], a Pontryagin's maximum principle is used to optimally update a model predictive control in each prediction horizon for an energy distribution task. The proposed MPC shows an improvement in the reduction in the total equivalent hydrogen consumption, saving up to 8.44% in the test case of FCEV while maintaining the stability of the battery SOC. In [21], a MPC based on a tailor-made mixed-integer linear programming optimization model was compared to a rule-based controller achieving a reduction in the energy consumed by at least 3.9% and up to 17.9%.

In offline approaches, heuristic algorithms highlight with the genetic algorithm (GA). In [22], Álvarez et al. implemented a GA that managed the hydrogen consumption based on the battery SOC level so that the battery had an optimal response matching the driver's power demand while the SOC level of the battery was maintained. Wiczorek et al. proposed two strategies in their work [23] two strategies, one incorporating fixed coefficients of a load power continuous function alongside other that uses the genetic algorithm (GAS) to optimize other coefficients in real-time with the backward time window. They manage to significantly decrease the charge and discharge currents of a LiFePO<sub>4</sub> battery module, thus extending its cycle life.

Finally, within artificial intelligence approaches, there are learning-based algorithms, which use large historical data set alongside real-time information to obtain an optimal control. Therefore, they are strategies with the capability to learn and adapt in order to achieve model-free control [24]. Artificial neural networks (ANNs), for example, were developed in [25], where an ANN is trained based on an optimal dynamic programming (DP) and achieve a network capable of producing near-optimal results that can be implemented in real time—unlike DP. Reinforcement learning, on the other hand, has also been studied in [26], where a model based reinforcement learning based on Q-learning was design maintain the SOC level of the battery near a reference while minimizing amount of hydrogen consumed. Compared to rule-based strategy, the hydrogen consumption decreased by 5.7% on average.

Based on the literature, it has been considered the RBC strategy as the most suitable for study since it is a strategy used in actual commercial FCEVs where the low computational cost stands out, with the non-necessity to have driving condition information. Moreover, more complex control strategies described before have not shown really significant improvements over RBC. We want to test that, even with a simple energy management algorithm, optimal results can be obtained with respect to hydrogen consumption and the battery level. Thus, in order to consolidate this control strategy, a rule-based operation mode control strategy for EMS has been proposed in this work with the aim of keeping the battery SOC at the same level while consuming as little hydrogen as possible.

The structure of this manuscript is as follows: Section 2 provides a description of the different systems that make up the hydrogen car such as the fuel cell or the battery and their specifications, as well as the topology chosen for the FCEV. Section 3 describes the control algorithm used for energy management and briefly describes the control used for the induction motor and the fuel cell. The results are shown in Section 4 where driving cycle tests, battery management tests, and a hill test were conducted. Major conclusions of the research performed are provided in Section 5.

## 2. Material and Methods

### 2.1. Topology

FCEVs share similarities in terms of drive train topology with battery electric vehicles (BEVs), wherein fuel cells act as the primary power source akin to batteries in conventional electric cars. However, unlike solid power sources, fuel cells exhibit limitations in promptly adapting to sudden load changes and state transitions, thereby lacking the benefits of regenerative energy storage [27]. Consequently, in commercial FCEV configurations, the integration of secondary energy storage devices such as super-capacitors or batteries alongside fuel cells is essential [28].

Based on [24], the powertrain of FCEVs can be divided into three categories: fuel cell and battery (FC + B), fuel cell and super-capacitor (FC + SC), and fuel cell, battery, and super-capacitor (FC + B + SC). Since the FC + B + SC configuration is complex and considering the low-energy density of super-capacitors, the FC + B configuration is the primary design choice and is utilized in the majority of FCEVs. Nevertheless, the FC + UC topology has been studied as in [29], where the topology was applied on a fuel cell electric tram. As Yan et al. explained, the operating conditions of the tram are different from other vehicles. Tram systems typically experience low average power demands but encounter spikes in power requirements during frequent start—stop operations, influenced by factors such as station settings. Consequently, and given its rapid charging and discharging capabilities, the super-capacitor emerges as a suitable choice for addressing the variable power demands of trams.

The complex FC + B + SC was studied by Paladini et al. [30] with the aim of optimizing the control strategy parameters in order to minimize fuel consumption while preserving the battery SOC based on genetic algorithms. Although the use of two secondary energy devices requires a more complex control strategy, they found out that the super-capacitor utilized a significant portion of the braking energy and therefore improved the fuel economy for the different driving cycles they tested.

Within the FC + B category, the most preferred configuration, due to its great flexibility in controlling the power flow for both FC and battery systems [31], is the one shown in Figure 1. Both PEMFC and battery are connected to the 400 V DC bus through a DC/DC converter in order to maintain 400 V in the bus and control the power provided by the fuel cell in the case of the battery and the PEMFC, respectively. From the bus, the induction motor powered through an inverter that provides the AC current that the motor needs to work. The DC bus also powers some other auxiliary devices like power steering, lights, fuel pump, air-conditioner, etc. As stated in [32], the consumption of the set is around 1.5 kW, which will be taken into account when carrying out the experiments.

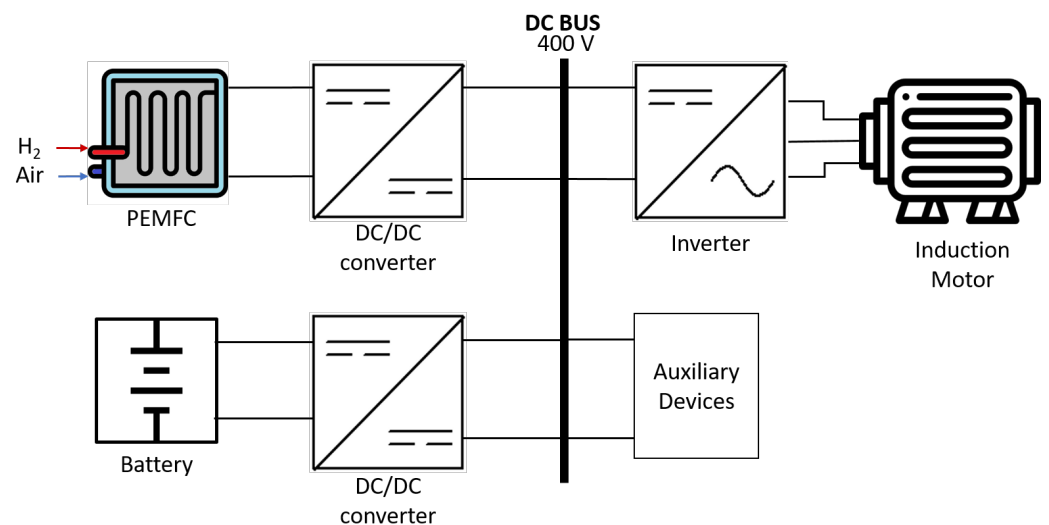


**Figure 1.** FC + B topology for a FCEV.



Focusing now on each element, as mentioned in the Introduction, the PEMFC is the device responsible for supplying electrical energy to both the induction motor and the battery using hydrogen by means of reverse electrolysis.

In the Figure 2, the work curves of the simulated PEMFC can be observed showing the relationship of the current with the voltage and the power. In relation to the power, a clear direct relationship can be observed, where the power provided by the fuel cell increases as the current does it too. In the graphs, two points of operation can be distinguished: the yellow one that represents the nominal operation point of the fuel cell at 50 kW and the orange one that represents the point of maximum power that the fuel cell can provide.

It should be mentioned that, as described in [33], the efficiency of the fuel cell decreases as the current increases since the voltage decreases as the current increases. This phenomenon will be taken into account when developing the energy control algorithm in Section 3 due to its high relevance.

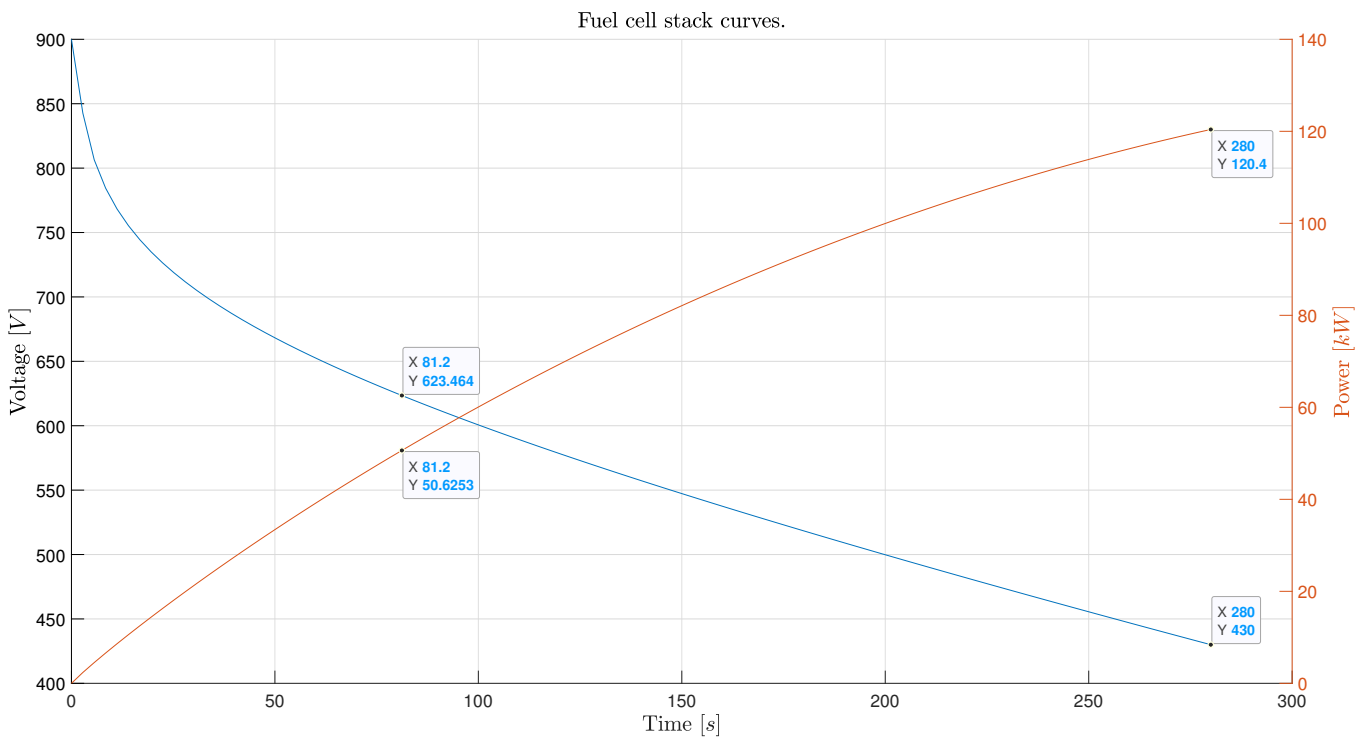


**Figure 2.** PEMFC characteristic curves.

The specifications of the PEMFC used in the simulation are presented in Table 1. It is worth mentioning that a PEMFC of these characteristics has been chosen on the basis of that described by Dimitrovar et al. [34], which differentiates between three different FC integrations: one where the FC becomes the main power supplier (100 kW) with a secondary battery (<2 kWh); another where the FC becomes a range extender being, which is a small power one (5 kW) together with a conventional electric car battery of more than 20 kWh; and a last one where the FC and the battery are of intermediate powers, about 45 kW and 10.5 kWh, respectively. This last configuration is the one chosen for this work as it shows advantages in terms of performance, durability, packaging, and cost.

**Table 1.** PEMFC specifications.

| Characteristic           |                  | Value | Unit  |
|--------------------------|------------------|-------|-------|
| Nominal operating point  |                  |       |       |
|                          | Power            | 50    | kW    |
|                          | Voltage          | 625   | V     |
|                          | Current          | 80    | A     |
| Maximum operating point  |                  |       |       |
|                          | Power            | 120   | kW    |
|                          | Voltage          | 430   | V     |
|                          | Current          | 280   | A     |
| Number of cells          |                  | 900   |       |
| Nominal stack efficiency |                  | 55    | %     |
| Nominal air flow rate    |                  | 2100  | L/min |
| Nominal supply pressure  |                  |       |       |
|                          | Fuel             | 1.5   | bar   |
|                          | Air              | 1     | bar   |
| Nominal composition      |                  |       |       |
|                          | H <sub>2</sub>   | 99.95 | %     |
|                          | O <sub>2</sub>   | 21    | %     |
|                          | H <sub>2</sub> O | 1     | %     |

Regarding to the induction motor (IM), the following Equation (1) describes its mechanical dynamics used as a model in order to develop the model predictive control used to control this IM as indicated in Section 3.

$$J \frac{d\omega_m}{dt} + B_v \omega_m + T_L = T_e \quad (1)$$

where:

$J$  = inertia coefficient (kg/m<sup>2</sup>)

$\omega_m$  = mechanical speed (rad/s)

$B_v$  = friction coefficient (Nms/rad)

$T_L$  = torque of the load (Nm)

$T_e$  = applied electromagnetic torque (Nm)

The specifications of the induction motor utilized in this study are detailed in Table 2.

The ion-lithium battery, on the other hand, plays a complementary role as mentioned before. It is used in combination with the PEMFC to provide additional energy storage and power backup. This allows for more efficient energy management and increased range, as the batteries can store energy during regenerative braking and release it when needed to further supplement the fuel cell power.

Following [35,36], the battery voltage while charging and discharging is described by the following Equations (2) and (3):

- Charging ( $i^* > 0$ ):

$$V_{\text{batt}} = E_0 - R \cdot i - K \cdot \left( \frac{Q}{it - 0.1 \cdot Q} \right) \cdot i^* - K \cdot \left( \frac{Q}{Q - it} \right) \cdot it + Ae^{-B \cdot it} \quad (2)$$

- Discharging ( $i^* < 0$ ):

$$V_{\text{batt}} = E_0 - R \cdot i - V_p - K \cdot \left( \frac{Q}{Q - it} \right) \cdot i^* + Ae^{-B \cdot it} \quad (3)$$

where:

$E_0$  = constant voltage (V)

$R$  = internal resistance ( $\Omega$ )

$K$  = polarization resistance ( $\Omega$ )

$Q$  = capacity (A)

$it$  = actual battery charge (Ah)

$i^*$  = filtered current (A)

$A$  = exponential zone amplitude (V)

$B$  = exponential zone time constant inverse ( $\text{Ah}^{-1}$ )

$V_p$  = polarization voltage ( $V_p = K \cdot (\frac{Q}{Q-it}) \cdot it$ )

**Table 2.** Induction motor specifications.

| Characteristic                  | Value                | Unit     |
|---------------------------------|----------------------|----------|
| Nominal frequency (fn)          | 68.4                 | Hz       |
| Nominal speed (Vn)              | 3800                 | rpm      |
| Maximum torque                  | 860                  | Nm       |
| Maximum power                   | $270 \times 10^3$    | W        |
| Power factor                    | 0.85                 |          |
| Pole pairs                      | 2                    |          |
| Stator resistance (Rs)          | 250                  | $\Omega$ |
| Rotor resistance (Rr)           | 0.7                  | $\Omega$ |
| Magnetizing inductance (Lm)     | $500 \times 10^{-6}$ | H        |
| Stator leakage inductance (Lls) | $19 \times 10^{-6}$  | H        |
| Rotor leakage inductance (Llr)  | $19 \times 10^{-6}$  | H        |

It is assumed that the internal resistance in the simulated battery is a constant throughout the charging and discharging cycle. It should also be mentioned that, in the discharging model, a term is described that concerns the polarization voltage to better represent the open circuit voltage (OCV) behavior.

In relation to the SOC, as stated in [37], it is described by the following Equation (4):

$$\text{SOC}(t) = \text{SOC}(0) - \frac{\int_0^t \eta i_m(\tau) d\tau}{C(\kappa)} \quad (4)$$

where:

$\eta$  = Coloumbic efficiency ( $\eta = 1$  for discharge, and  $\eta < 1$  for charge)

$i_m(\tau)$  = battery measurement current in  $\tau$  instant (A)

$C(\kappa)$  = total available capacity (Ah)

$\kappa$  = charge–discharge rate ( $\kappa = |i|/C_n$ )

$C_n$  = nominal capacity (Ah)

As mentioned before, in Section 1, the aim of the control algorithm is to maintain the battery SOC level as much as possible; thus, the remaining useful life (RUL) of the battery is extended. This allows delaying the adverse effects of aging of Li-Ion batteries described in [38] that affects the safety behavior of the cells. This paper also discusses the importance of the temperature to which the battery is subjected and how it affects degradation. In other work [39], Wang et al also discussed the role of temperature on the voltage plateau behavior value and its importance. However, although temperature exposure is of great relevance, it is not a variable that enters into our control algorithm since our objective is only to maintain the SOC level.

The specifications of the ion-lithium used in this work is described in Table 3. As with the PEMFC, the capacity of the battery has been chosen based on the topologies described in [34]. As mentioned before, a middle-range power fuel cell and capacity battery are used in this work—specifically, a battery of 30 Ah or 12 kWh specifically.

**Table 3.** Lithium-ion battery specifications.

| Feature                     | Value          | Unit     |
|-----------------------------|----------------|----------|
| Parameters                  |                |          |
| Type                        | Lithium-Ionion | -        |
| Nominal voltage             | 400            | V        |
| Rated capacity              | 12             | kWh      |
| Battery response time       | 30             | s        |
| Discharge                   |                |          |
| Cut-off voltage             | 300            | V        |
| Fully charged voltage       | 465.59         | V        |
| Internal resistance         | 0.04           | $\Omega$ |
| Capacity at nominal voltage | 1.08           | kWh      |

## 2.2. Drive Train

Despite modeling the induction motor, other aspects of the motor have to be taken into account in order to be able to perform tests equivalent to those of a real car. All of the car specifications used for the car modelling are shown below in the next Table 4.

**Table 4.** FCEV car specifications.

| Characteristic                     | Value             | Unit              |
|------------------------------------|-------------------|-------------------|
| Weight                             | 2250              | kg                |
| Maximum speed                      | 250               | km/h              |
| Wheel diameter                     | 0.7               | m                 |
| Gear ratio                         | 9.73              |                   |
| Braking force                      | $20 \times 10^3$  | N                 |
| Regenerative braking minimum power | $-60 \times 10^3$ | N                 |
| Transmission efficiency            | 0.96              |                   |
| Front Area                         | 2.1               | m <sup>2</sup>    |
| Drag coefficient                   | 0.24              |                   |
| Rolling coefficient                | 0.025             |                   |
| Inertia coefficient                | 1.2               | kg/m <sup>2</sup> |

Based on the equation of the mechanical model described in the Section 2.1, a simpler form can be defined (Equation (5)).

$$\frac{dw_m}{dt} = \frac{1}{J}(T_e - B_v w_m - T_L) \quad (5)$$

In this mechanical model, the load torque term can be described as the sum of torques generated by the car brakes and the gradient, rolling, and wind resistance, as described in Equation (6). These terms, described in [40], are among the most relevant components

within the road loads, taking into account the fact that no curves were simulated in the experiments carried out.

$$T_L = T_{brake} + T_{gradient} + T_{rolling} + T_{wind} \quad (6)$$

In order to obtain the torque generated by the road load resistances, the force must be first be obtained following Equations (7)–(9). In a next step, Equation (10) is used with each term, thus achieving the torque.

$$F_{gradient} = m_{car} * \sin(\alpha_{hill}) \quad (7)$$

$$F_{rolling} = m_{car} * c(v_c) \quad (8)$$

$$F_{wind} = \frac{1}{2} * \rho_{air} * c_d * S_{front} * v_c^2 \quad (9)$$

$$T_x = \frac{D_w/2}{i} F_x \quad (10)$$

where:

$m_{car}$  = car weight (Kg)

$\alpha_{hill}$  = hill angle (rad)

$c(v_c)$  = rolling coefficient based on car speed

$\rho_{air}$  = air density (kg/m<sup>3</sup>)

$c_d$  = drag coefficient

$S_{front}$  = front area of the car (m<sup>2</sup>)

$v_c$  = car speed (m/s)

$D_w$  = wheel diameter (m)

$i$  = gear ratio

$T_x$  = torque generated by x term (Nm)

$F_x$  = force generated by x term (N)

In the case of car brakes, since the modeled car is considered a non-human driven car, an algorithm is designed to control the torque generated by the brakes. As shown in [41], different strategies could be implemented depending on the relationship of the car brakes and the motor regenerative braking. In this work, the so-called series control strategy is used, where the motor is used to brake the vehicle and regenerate the battery. If the motor is not able to provide the requested torque, car brakes are used to complete the task.

It should be noted that the described strategy is only running when the energy management control, based on the state of charge (SOC) of the battery, allows for regenerative braking.

### 3. Control Strategies

Before describing the different control strategies used for each system, a diagram block is presented in the next Figure 3 that corresponds to the generic control scheme of all subsystems.

Based on color, the next description is given:

- Blue: model of the induction motor and inverter, alongside the drive train described before.
- Orange: model of both battery and PEMFC including both DC/DC converters.
- Yellow: subsystems that host the control algorithm for each element: battery and PEMFC converters, induction motor, and energy management.
- Green: subsystems that obtain measurements needed for the control algorithms.

It should be mentioned that an additional element is implemented in the diagram, named auxiliary devices. As explained in Section 2.1, the DC bus also powers some other



auxiliary devices like power steering, lights, fuel pump, air-conditioner, etc. and the consumption of all is set to a constant of 1.5 kW.

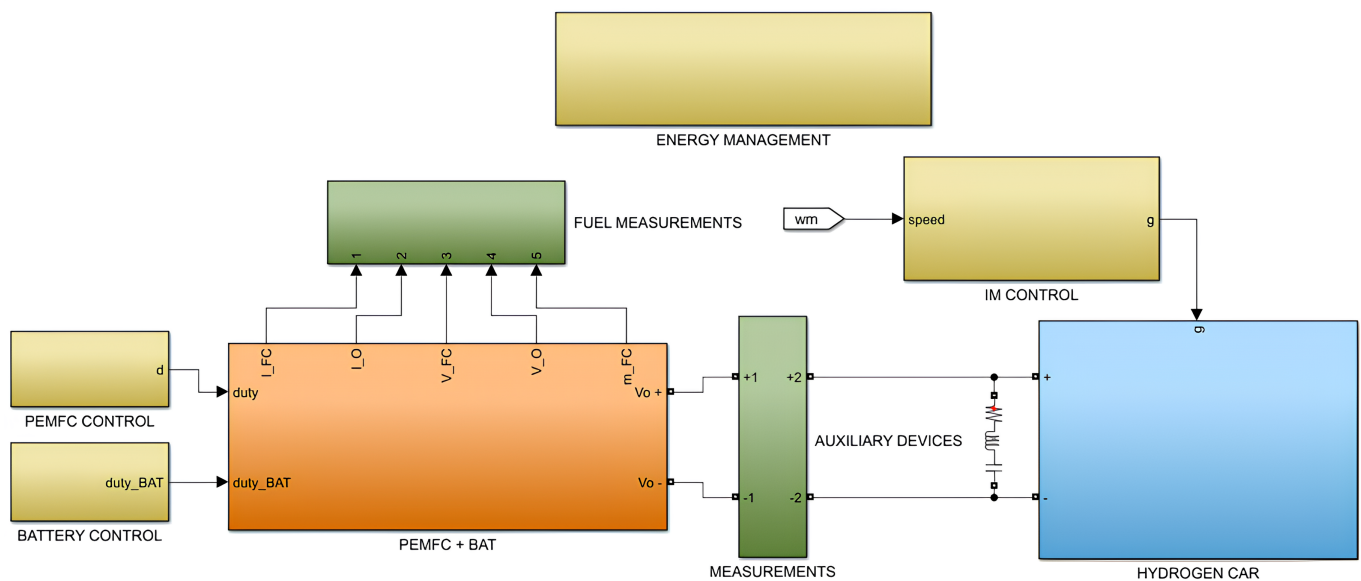


**Figure 3.** Control scheme of the FCEV.

### 3.1. Rule-Based Energy Management

In this work, as stated in Section 1, a simple RBC is designed to test whether a simple algorithm of energy management is capable of achieving optimal results with respect to hydrogen consumption and the battery SOC level under real driving conditions, as it will be discussed in the next Section 4. These results, could lead to the industrial application of the designed EMS since a rule-based EMS can be implemented on low-cost and low-power micro controllers due to the low computational cost of the algorithm. A RBC also shows a high robustness in all different scenarios as opposed to optimization- or learning-based algorithms [24], thus aligning with the conservatism of the automotive industry where, as mentioned in the introduction, rule-based algorithms are the preferred choice.

Obviously, a more complicated energy management control scheme based on artificial intelligence or deep learning could be designed; however, the applicability of these control schemes requires a high computational cost and its robustness under unexpected situations is difficult to evaluate. Therefore, its utilization in the automotive industry for a real vehicle would be more difficult.

A rule-based optimization method is a technique used in energy management to make optimal decisions on how to manage and use the available energy in a system, in our case, a FCEV. Instead of relying on complex algorithms or predictive models, rule-based optimization is based on a set of predefined rules that guide the behavior of the system in different situations. Therefore, the low computational cost is achieved when the RBC is implemented.

Based on an operation mode control strategy discussed in [42], also called the multi-mode strategy in [29], different states are fed into the rule-based algorithm. In our case, three states are implemented: traction state, braking state, and stationary state. In the first one, the motor demands power, while in the second one, the motor provides energy to the bus. In the stationary state, the demanded power by the motor is zero.

Apart from states, the battery SOC is also fed to the rule-based algorithm, as shown in Figure 4. In order to maintain the RUL of the battery, the SOC is taken into account in the algorithm. Later in this section, when fully describing the algorithm, the SOC sections chosen and applied to the control will be explained.

As can be observed, the output of the algorithm corresponds to the output power that the fuel cell has to provide to the DC bus and a signal that allows regenerative braking (RB).

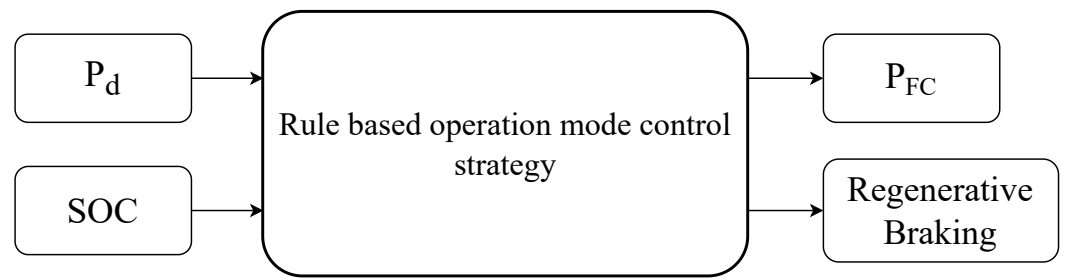


**Figure 4.** Rule-based strategy general scheme.

In the next Figures 5–7, the control algorithm for each mode is presented. As can be observed, after knowing the mode of operation, the algorithm observes the SOC of the battery and based on the section it is in, a reference power value for the fuel cell is given. In the braking state, a regenerative braking command is also given to activate or deactivate this function.

Battery SOC sections are divided based on critical point: points—20 and 80%—from which the SOC should not go down or up, respectively, in order to increase the RUL of the battery. Furthermore, as mentioned in [43], the lifetime of batteries is improved through the minimum variation of SOC, and thus, a SOC range between 50 and 80 is also implemented in the control algorithm. Moreover, if the SOC allows it, PEMFC is always the first choice to power the motor, avoiding having to charge the battery first and then power it throughout the batteries. This is due to the fact that there are more components involved in powering the motor, which implies more component power losses.

The main purpose of the algorithm, as will be observed, is to maintain the battery SOC between 50% and 80% while consuming as less hydrogen as possible. This is obtained by giving different power commands to the fuel cell low level control system, i.e., commands to work in different modes:

- $P_{FC} = P_{Max}$ : the output power of the fuel cell is the maximum possible. This mode is only used when the battery SOC level is below 20%.
- $P_{FC} = P_d$ : the output power of the fuel cell is equal to the demanded power required by the motor and the auxiliary devices ( $P_d$ ). Therefore, the battery is not charging and the SOC level is maintained during this mode.
- $P_{FC} = P_{Eff}$ : as described in Section 2.1, the efficiency of the PEMFC decays as the current and the power increases. Therefore, it is considered an efficiency mode to meet the demanded power in the tightest way, but has the ability to slightly charge the battery. Thus, the efficiency power is given by the next Equation (11):

$$P_{Eff} = P_d + 1 * 10^4(W) \quad (11)$$

Sometimes, in this mode, it can occur that the demanded power can exceed the  $P_{Max}$  of the fuel cell. In that case, the  $P_{Eff}$  is equal to the maximum power possible.

- $P_{FC} = P_{Aux}$ : the fuel cell output power is only set to power only the auxiliary devices.
- $P_{FC} = 0$ : the PEMFC is in an idle situation where zero hydrogen is consumed, and thus, zero power is given to the DC bus. The battery has to provide all the energy requested by the motor and the auxiliary devices.

As mentioned before, the SOC of the battery should remain between 50% and 80%. In the traction state, the power provided by the PEMFC decreases as it reaches this range. Thus, as shown in Figure 5, it delivers a maximum power below 20%, enters the efficiency mode between 20% and 50%, and matches the demanded power between 50% and 80%. Beyond that limit, the fuel cell enters the idle mode with zero output power and zero

hydrogen consumption. Therefore, an energy management is implemented with the aim of maintaining the SOC is implemented.

In the braking state, the regenerative braking (RB) command is applied, as shown in Figure 6. This RB is always activated, and in braking state, it is the main power source to charge the battery. In order to elongate the RUL of the battery, RB could be deactivated when the SOC is above 80% and the battery would not charge; however, the energy would be wasted and the normal brakes would have to apply more force. Thus, the choice of this function is relegated to the driver. For the subsequent experiments, it has been assumed that the driver has decided not to activate the regenerative braking after 80% of SOC.

With regard to the FC, only when the SOC level is between 20% and 50%, does the FC provide the power demanded by the auxiliary devices. Therefore, all the power of RB is provided to the battery. At higher SOC values, the FC provides no energy and the RB has to power the auxiliary devices while charging the battery.

In stationary state, if the battery SOC exceeds 50%, the fuel cell does not provide any power and the battery has to power auxiliary devices. Between 20% and 50%, the PEMFC provides enough power to charge the battery while powering the auxiliary devices as it is in efficiency mode. Below 20%, following the previous modes, the fuel cell works at maximum power in order to raise the SOC level.

It should be mentioned that, in traction state, when a big acceleration is demanding, i.e., the power demand rises above the fuel cell maximum output power, the battery and PEMFC work together in order to provide all the needed energy. Nevertheless, if the battery is below 20%, since such low levels of SOC have must be avoided, the power demanded by the motor is limited to the maximum power that the fuel cell can provide following the next Equation (12). It should be observed that a gain of 0.85 is added in order to have enough power left to charge the battery.

$$P_{trac} = P_{FC} * 0.85 \tag{12}$$

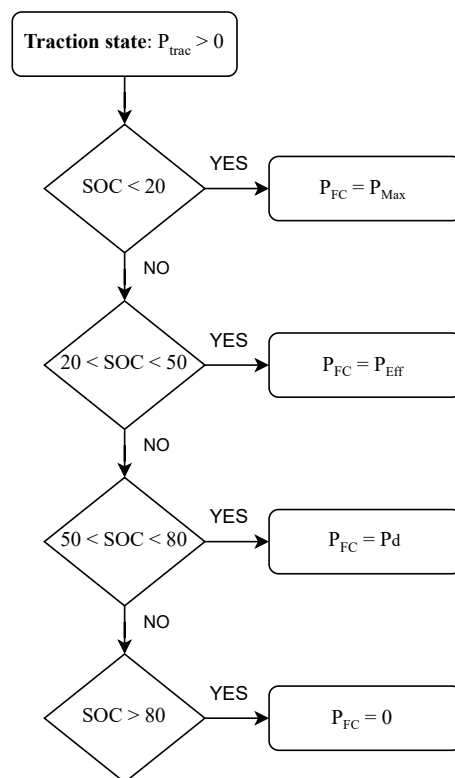


Figure 5. Traction state decision tree.

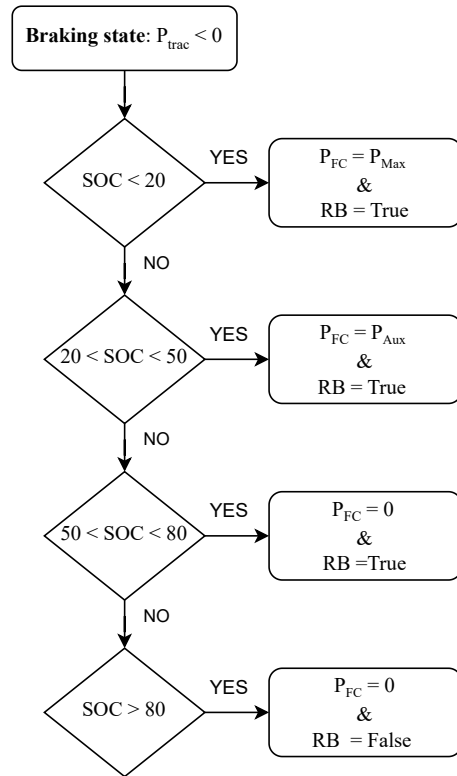


Figure 6. Braking state decision tree.

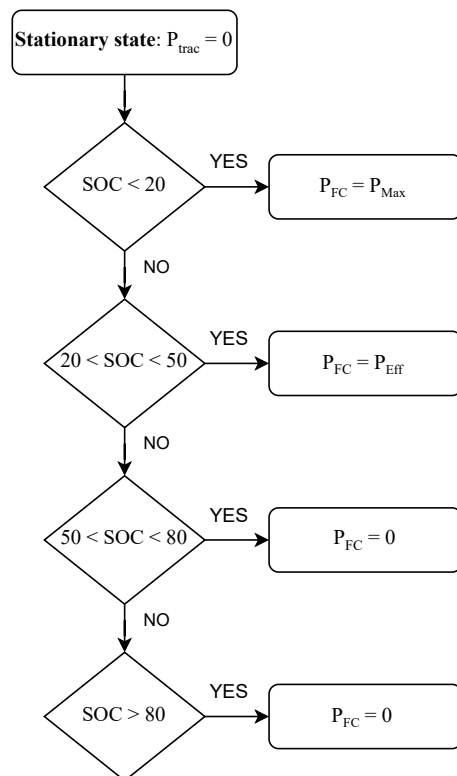


Figure 7. Stationary state decision tree.

### 3.2. Fuel Cell and Battery

Both PEMFC and battery stack are connected to the DC bus by means of DC/DC converters. In the case of PEMFC, a DC/DC buck converter is used in order to control the output power of the fuel cell and match the energy needs controlled by the higher-level

energy management control described above. The relationship between input and output voltage in a buck converter is regulated by the switch duty cycle,  $d$ , as expressed in the following Equation (13). As  $d$  must always be lower than one,  $V_{out}$  is also lower than  $V_{in}$ .

$$V_{out} = d * V_{in} \tag{13}$$

When it comes to control the duty cycle of the buck converter, different controllers are used based on the mode chosen by the rule-based energy management described in the previous subsection. When  $P_{Max}$  is needed, a simple perturb and observe (P&O) is used to look for the maximum power. On the other hand, when  $P_{Eff}$ ,  $P_d$ , or  $P_{Aux}$  is needed, as they are based on error, a PID controller is implemented with the following values (Table 5).

**Table 5.** Design parameters for the PID used in buck converter.

| Parameters | $K_p$ | $K_i$ | $K_d$ |
|------------|-------|-------|-------|
| Values     | 0.002 | 0.01  | 0     |

On the other hand, in the case of the ion-lithium battery, a bidirectional DC/DC converter is used in order to always maintain the 400 V value of the DC bus needed for the induction motor and its control to correctly work. The relationship between the input and output voltage is regulated by the switch duty cycle,  $d$  as expressed in the following Equation (14). In this case,  $V_{in}$ , i.e., battery voltage is considered the low-voltage (LV) side of the converter, and  $V_{out}$ , i.e., bus voltage is considered the high-voltage (HV) side.

$$V_{out} = \frac{1}{1 - d} * V_{in} \tag{14}$$

In order to obtain a suitable value of duty cycle to maintain 400 V, the following PID-based control diagram has been implemented (Figure 8). As can be seen, a reference of 400 V is compared to the actual DC voltage and the error is then fed to the PID that regulates the duty cycle. A PWM generator is used to generate the gate signals from the duty cycle that are used to control the switches. It should be mentioned that the two switches  $S1$  and  $S2$  work alternatively, and thus, a NOT block can be observed in the diagram.

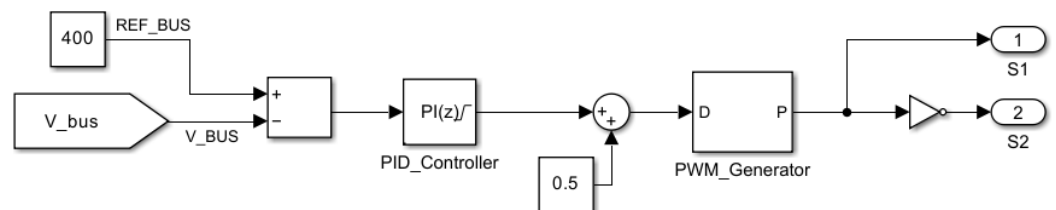


**Figure 8.** Bidirectional DC/DC converter control scheme.

### 3.3. Induction Motor FOC

Several points could be discussed with regard to the control of the induction motor, but as this is not the scope of the paper, it will be briefly described due to its relevance in the performance of the FCEV.

In a general induction control scheme (Figure 9), a speed control loop (magenta) and a lower-level current control loop (yellow) are distinguished. In the first one, the induction motor speed is fed back to a controller (a MPC in our case) and gives a reference torque signal to the current control loop. Here, a field oriented control (FOC) is applied and turns the torque signal into three phase sinusoidal signals that are fed into a sinusoidal pulse width modulation (SPWM) in order to obtain the six gate control signals of the inverter. This device lastly transforms the power in DC of the bus into AC that feeds the induction motor.



FOC is an advance control technique that allows for the independent control of two key aspects of the motor: the magnetic flux and the torque. In order to achieve it, the motor's actual three-phase currents are converted into a rotating reference frame (d-q frame) based on the rotor's position, where the d and q currents directly control flux and torque, respectively. Then, a reverse conversion is applied and the three-phase currents are obtained. It should be noted that FOC needs, alongside the torque reference, the FOC needs the measurement of three phase currents of the stator in order to work, as can be seen in Figure 9.

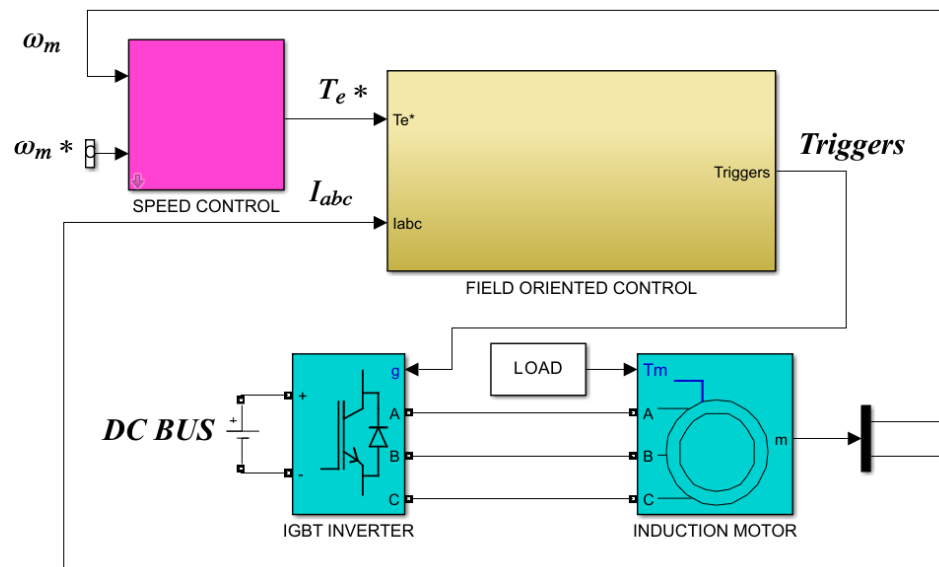


Figure 9. Induction motor control scheme.

#### 4. Results

Previously to discussing the results, it should be noted that the hardware used to run the simulations is a Dell Precision Tower 3420 (Warszawa, Poland) with an Intel(r) Core(TM) i7-6700 CPU at 3.4 GHz and 32 GB of RAM installed. Later, in the results section, it will be discussed the simulation time will be discussed and the step time chosen due to its limitations. The experiments were carried out using SIMULINK v10.6 from Matlab R2023B, where the block diagram and the control algorithm were implemented.

##### 4.1. Driving Cycles

As first experiment, the FCEV has been tested on the new European driving cycle (NEDC) in order to observe a general battery management and fuel consumption. This type of test provides standardized data on the fuel consumption and emissions of the vehicles, allowing consumers to compare efficiency between different car models [44]. In our hydrogen car, performing emission measurement has no sense since it is a zero emission vehicle; thus, consumption is the only variable to be observed.

The newer worldwide harmonized light-duty test cycle (WLTC) is the one used nowadays in the car industry to show the fuel economy of a car; however, as discussed in [45], the difference between the fuel economy obtained in the WLTC and NEDC depends on several factors, including vehicle technology, so neither test is reliable in terms of fuel economy. Moreover, a large share of the negative acceleration appears in the WLTC, giving greater opportunity to recover energy from regenerative braking in EVs, and thus improving the fuel economy of this type of vehicle compared to other more conventional ones such as ICE vehicles. Therefore, both driving cycles have been tested so fuel savings and SOC variation can be compared.

The NEDC presents a speed profile shown in Figure 10 where the performance of the designed FCEV can be observed. Of the total of 1180 s, the first 780 s are considered urban

driving cycles (maximum speed 50 km/h) and the next 400 s are the extra-urban driving cycles (maximum speed 120 km/h).

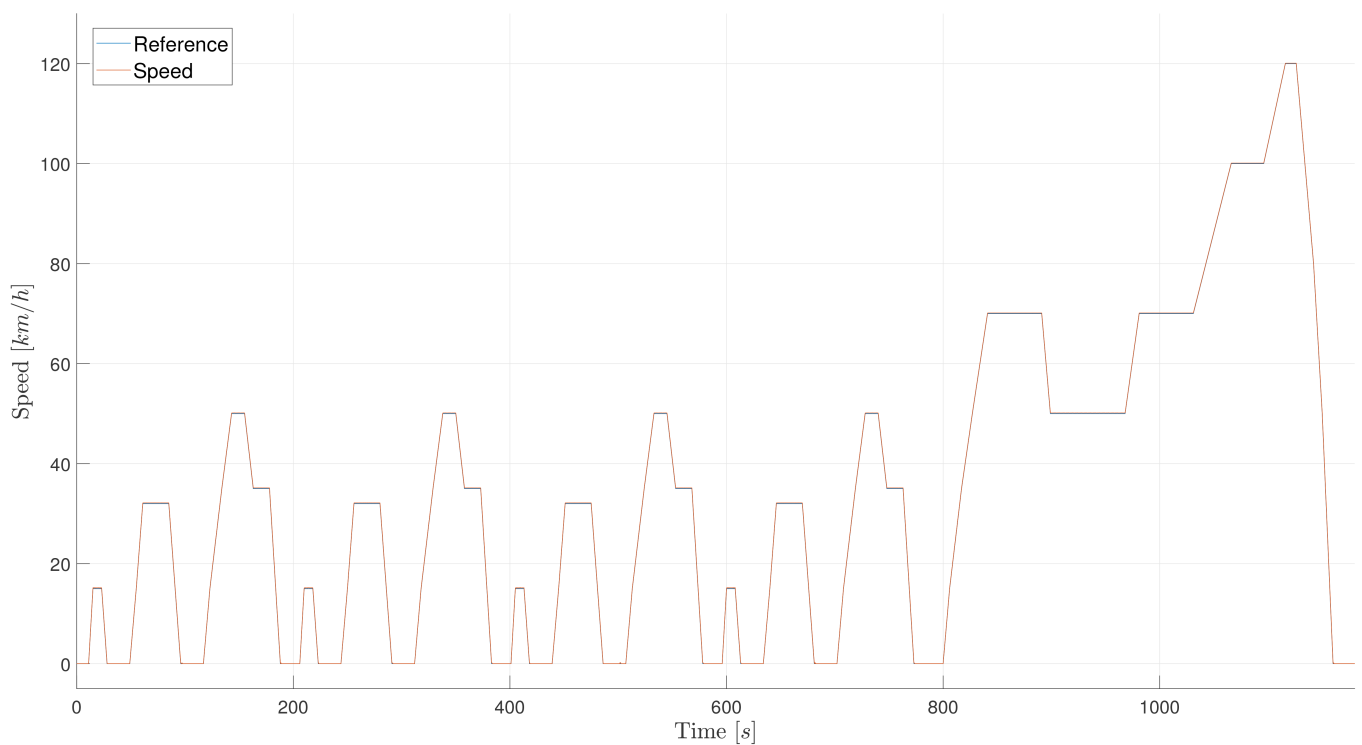


**Figure 10.** Speed performance of the FCEV during the NEDC.

Observing Figure 11, the demanded power required by the IM and the auxiliary devices during the NEDC can be known, alongside the output power of the FC and the battery power. It can be seen that the demanded power is always supplied by the fuel cell. The speed increases are not sufficiently abrupt to require the combined power of the FC and the battery, and, since the SOC level is in the optimal frame, the battery is not used.

It should be noted that, when the car is decelerating, it does it so slowly that, the motor does not demand negative power; demanding less power is sufficient to decelerate the car following the reference. Only when the speed reference needs for a substantial braking, the regenerative braking works as can be seen in the last speed drop at second 1120. In such cases, the PEMFC does not provide any power and the auxiliary devices are powered by the regenerative braking. Moreover, when the car is stopped, the PEMFC does also not provide any power either, so the battery pack supplies the demanded power, which only consists of the auxiliary devices.

In the last Figure 12, the SOC level and the hydrogen consumption during the NEDC is presented. As can be seen, the SOC remains between 65% and 63% throughout the test. This is due to the FC work, which always supplies the demanded power while the car is in traction mode ( $P_d > 0$  &  $v \neq 0$ ). The battery only drops when the car is stopped and the battery pack supplies the auxiliary devices. The hydrogen consumption, on the other hand, is only constant when the FC stops providing power; otherwise, hydrogen is always consumed. Thus, the NEDC test ends with a hydrogen consumption of 1.2 kg/100 km.

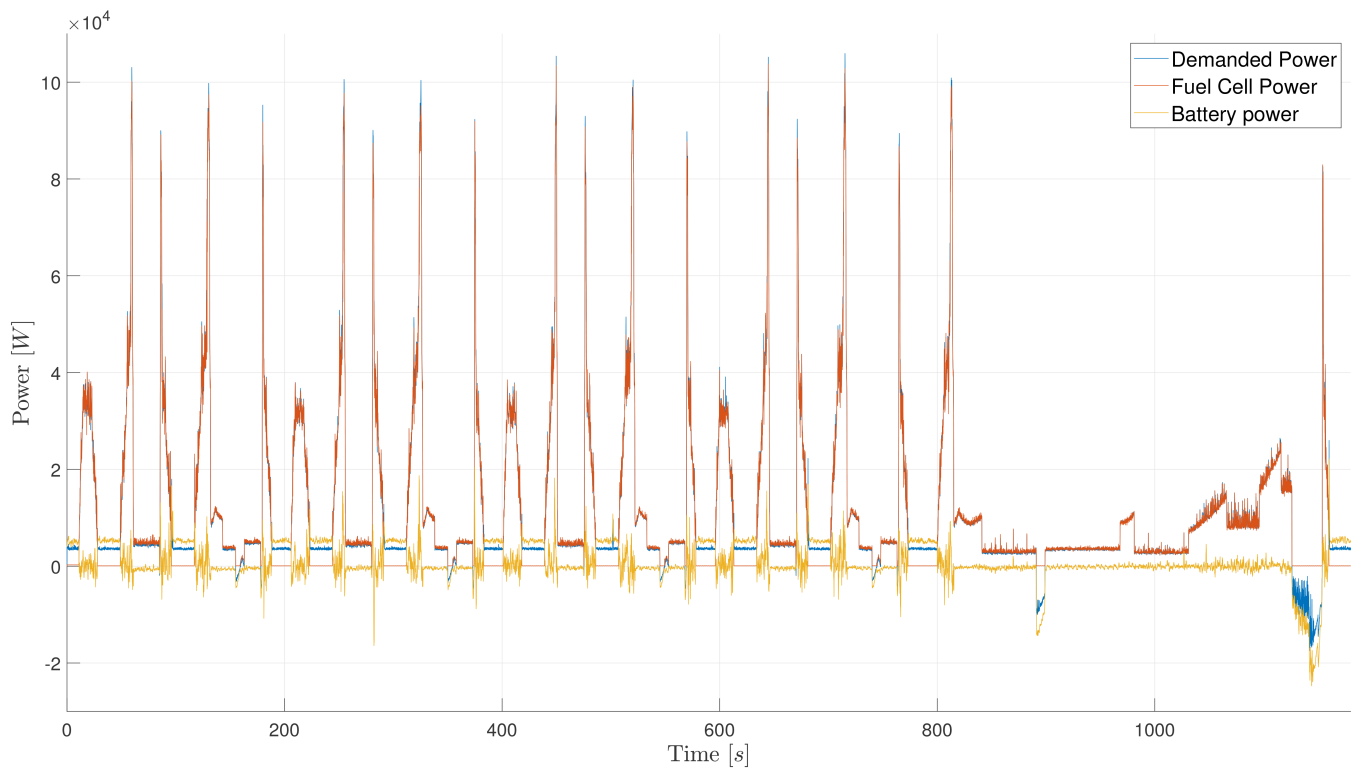


Figure 11. Demanded power, fuel cell power, and battery power during NEDC.

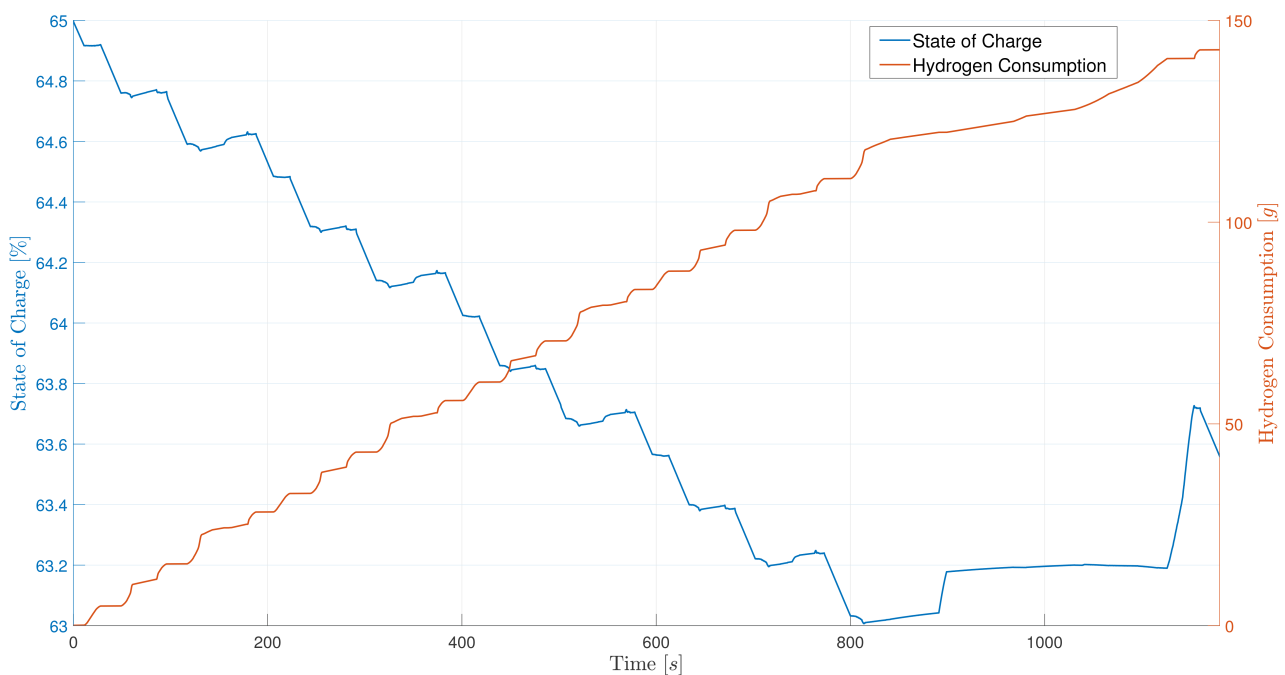
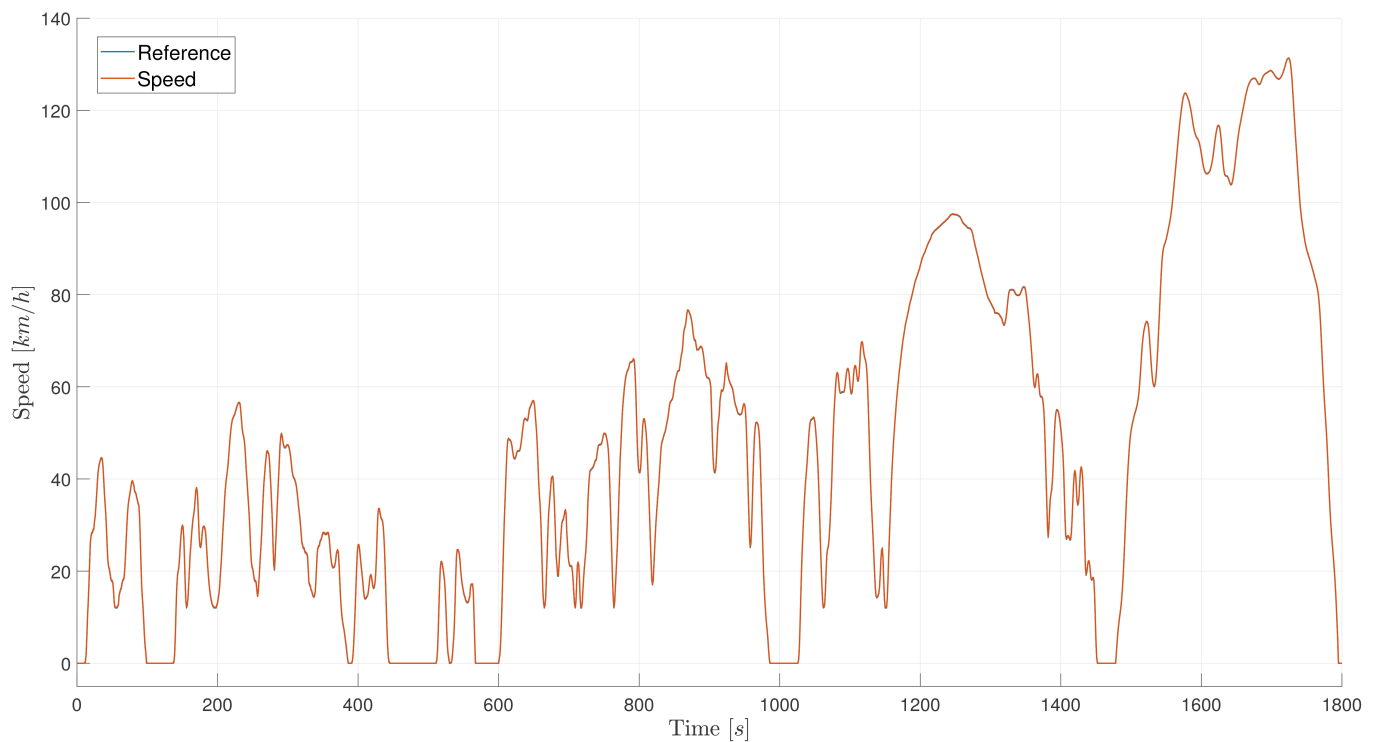


Figure 12. SOC and hydrogen consumption during NEDC.

In the case of WLTC, the class 3b type driving test has been selected since the FCEV reaches speeds beyond 130 km/h. In Figure 13, the speed performance of the vehicle during the test is shown. The driving cycle is based on four sections of low, medium, high, and extra high speed with 589, 433, 455, and 323 s of duration each, respectively.



**Figure 13.** Speed performance of the FCEV during the WLTC.

As the previous driving cycle, the Figure 14 is presented in order to compare the demanded power by the IM alongside the auxiliary units and the power provided by the FC and the battery during the test. As can be observed, the FC can always provide the demanded power so, in the most part of the test, battery power is oscillating around a value of zero. Only when the car is fully stopped is the battery responsible for providing the power demanded by the auxiliary devices. Compared to the NEDC, more regenerative braking has been used since the demanded power enters the negative region 3.2 times more.

In Figure 15, the variation of the SOC and the consumed hydrogen during the driving cycle is shown. The presented results are consistent with the previous Figure 14. The fact that the FC provides the demanded power most of the time, results in a maximum variation of the battery SOC of 1.24%. The generative braking also allows one to end up with only 0.45% less SOC. This results states what has been described above, specifically that WLTC shows better results in terms of battery consumption compared to the NEDC due to the amount of negative acceleration sections.

In the case of hydrogen consumption, the fuel consumed in WLTC is 1.7 times more than that of NEDC. This is due to the time during which the car is fully stopped, which is 1.2 less compared to the NEDC and the duration of the test itself, since it is a 620 s larger test. Nevertheless, the mean hydrogen consumption in 100 km is 1.07 kg which is 0.13 kg less compared to the NEDC.

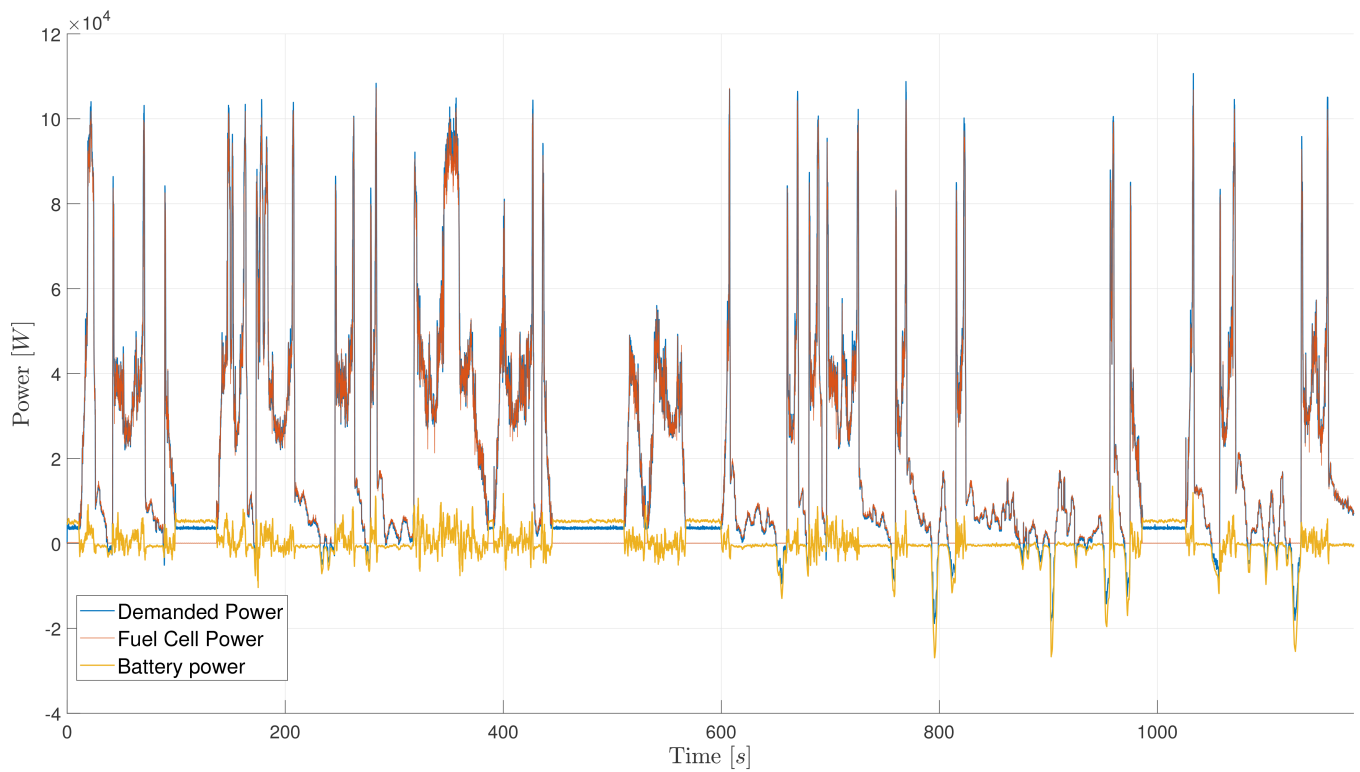


**Figure 14.** Demanded power, fuel cell power, and battery power during WLTC.

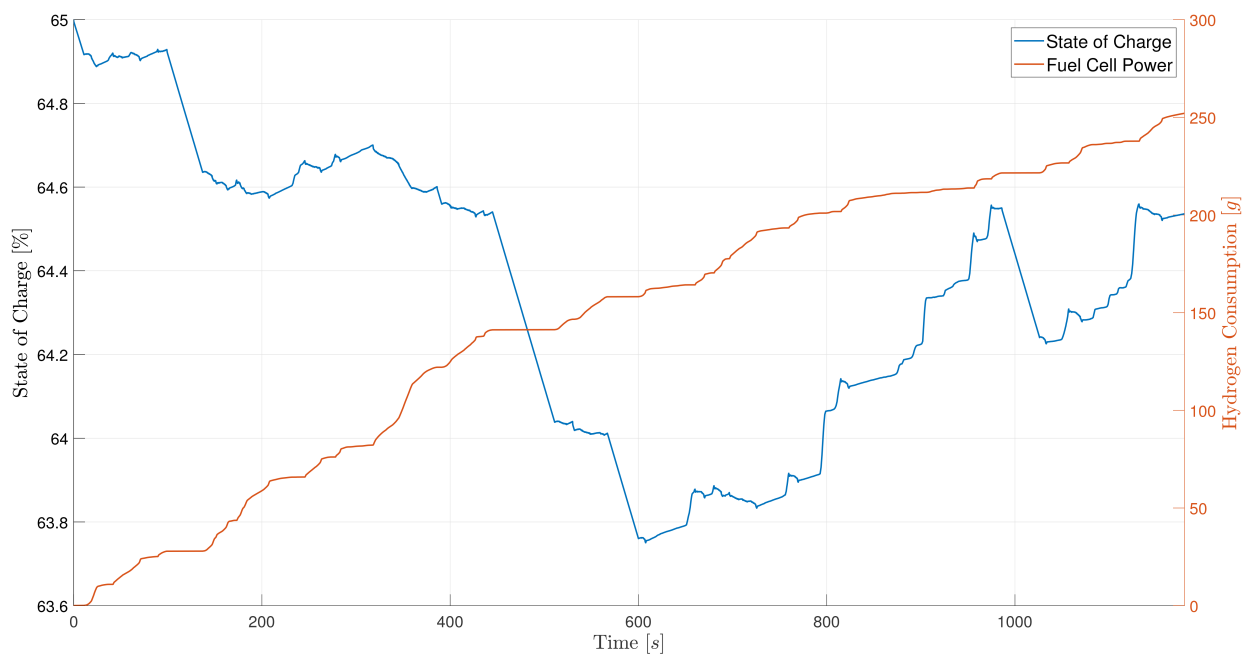


**Figure 15.** SOC and hydrogen consumption during WLTC.

#### 4.2. Battery Tests

In order to validate the energy management control, experiments at different operating points were conducted.

In the first case, the battery SOC level starts at 19.5%, near the boundary of the next SOC section from 20% to 50%. In the Figure 16, the speed of the FCEV and the reference



that follows are shown. A reference which allows one to surpass the 20% limit and see the performance of the energy management control is used.

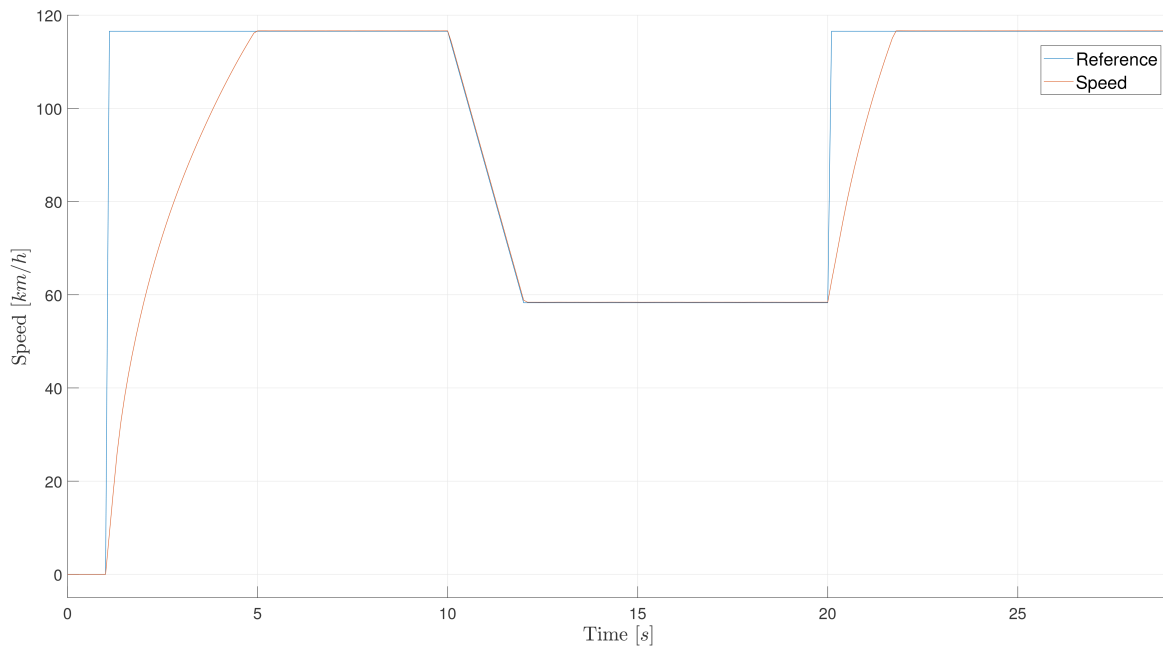


**Figure 16.** Speed performance of the FCEV with 20% of % SOC.

In the Figure 17, the SOC of the battery and the control commands of the energy management control are presented in order to observe the dependence of the battery pack on the control algorithm. As can be seen, the control commands are given by numbers which represent the different working modes described in Section 3. The following Table 6 matches the numbers used with the mode in which the FC operates.

**Table 6.** Control commands description.

| Control Command | 0                  | 1              | 2                  | 3            | 4                  |
|-----------------|--------------------|----------------|--------------------|--------------|--------------------|
| Mode            | $P_{fc} = P_{max}$ | $P_{fc} = P_d$ | $P_{fc} = P_{Eff}$ | $P_{fc} = 0$ | $P_{fc} = P_{Aux}$ |

Following Figure 17, it can be seen that until reaching 20% SOC in traction mode, the fuel cell offers the maximum possible power in order to pass this limit of 20% as soon as possible. Just after passing this limit, the fuel cell goes into efficiency mode to provide the power demanded and a little more to charge the battery. When the car needs to decelerate, in second 10, the regenerative braking activates and the battery only powers the auxiliary devices, thus increasing the rate of battery charging.

As can be seen, the overall objective of the algorithm is to bring the battery SOC above 50% by doing as much as possible to keep it above 20%. It is only when too much acceleration is demanded that the battery is combined with the fuel cell and the SOC is reduced, as in second 20. However, this is not the case for the first acceleration of the car at second 1, where the SOC value remains very close to the initial value of 19.5%. This is due to what was explained in Section 3.1 above: when the SOC is below 20%, the maximum torque of the motor is limited by the maximum power that the battery can deliver, so it adapts and does not have to rely on battery power.

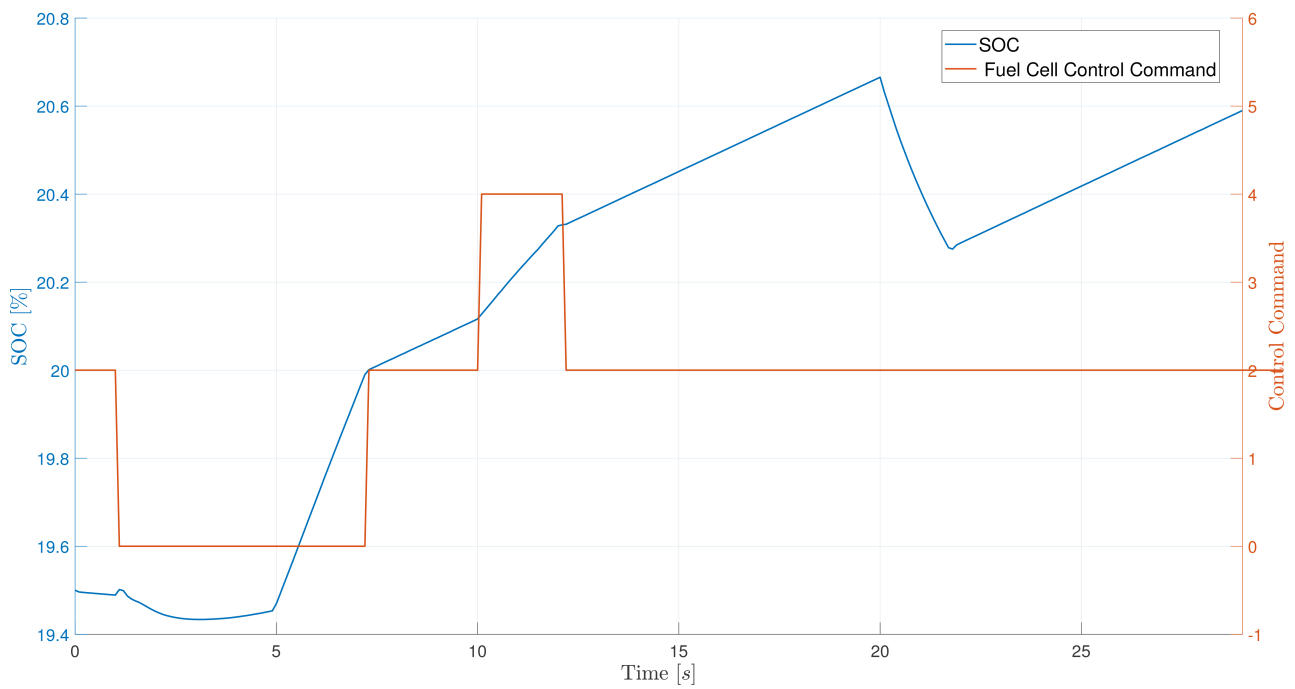


**Figure 17.** Control command and evolution of battery SOC whitwith 20% SOC.

In a second test, a SOC value close to the next 50% limit was chosen, which marks a new SOC section between 50% and 80%. As in the previous test, the aim is to observe the behavior of the energy control algorithm at a key operating point. Figure 18 below shows the speed profile chosen as a reference and the speed of the car.

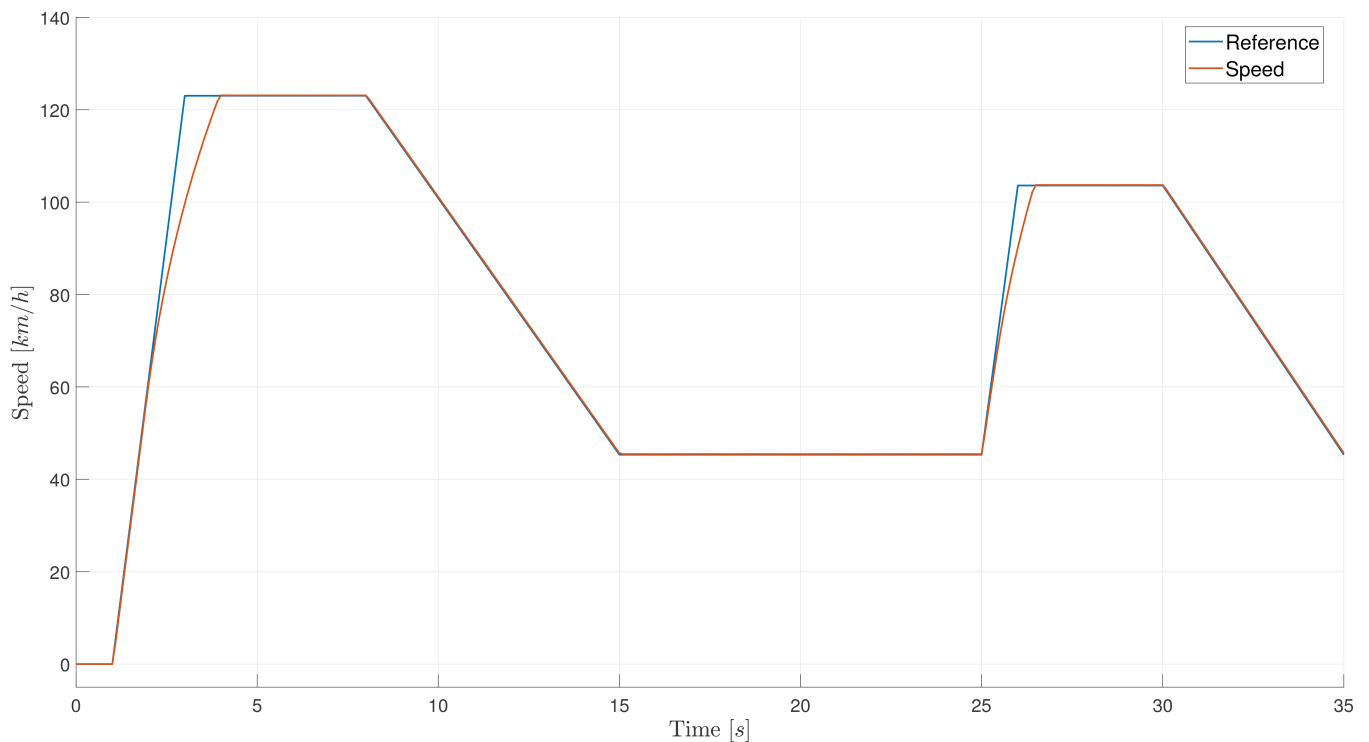


**Figure 18.** Speed performance of the FCEV with 50% of % SOC.

As before, Figure 19 shows the SOC of the battery and the control actions given by the energy controller. In this case, the SOC starts at 49.8% and reaches a value of 50.4% at the end of the test, following the target of the control algorithm to reach the 50–80 SOC section. In the two accelerations of seconds 1 and 25, as in the previous test, the power demand is provided by the combination of the battery and the FC reducing the SOC level. In these sections, the fuel cell is in efficient mode trying to recharge the battery while powering the IM. However, at the beginning of the second acceleration, the battery is at 50%, so the battery is in mode 1—providing exactly the power demanded without charging the battery. However, during the acceleration, the SOC goes back below 50% and the fuel cell returns to efficiency mode in order to recharge the battery.

In the braking state, when attempting to decelerate the car, the regenerative braking is active at all times and the fuel cell, depending on the SOC, goes into different modes of operation. In both instances of deceleration, the battery is charged and runs through the SOC 50% point, so the control algorithm switches from using the fuel cell power to feed the auxiliary elements (mode 4) to providing no energy at all (mode 3). It should be noted that this mode change shows no apparent change in the battery SOC as the auxiliary elements only consume 1500 W, which is negligible compared to the regenerative capacity of the engine.

Finally, a test with a SOC level of around 80% is presented. In Figure 20, the speed reference and the actual speed of the vehicle during the test is shown. Compared to the previous tests, a profile has been chosen where a slower rising speed gradient appears, so that the control action can be observed in that state being very close to 80% of % SOC.

In Figure 21, it can be seen the SOC of the battery and the control algorithm's choice of fuel cell operating mode are shown. The first thing to note is that, above 80%, the battery never contributes power to the DC/DC bus as the SOC must be kept below that 80% limit. Below that point, in traction state, the battery provides exactly the power demanded, and hence the SOC remains constant. In braking state, on the other hand, the battery remains in mode 3, i.e., without consuming hydrogen.

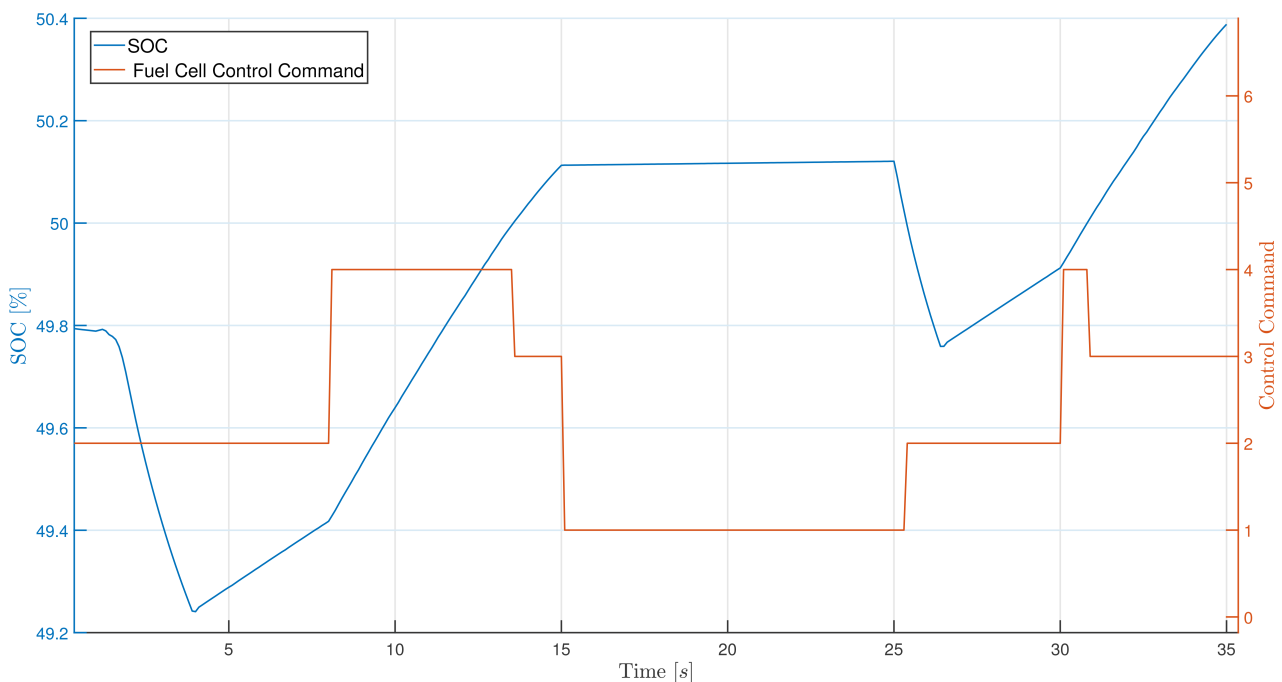
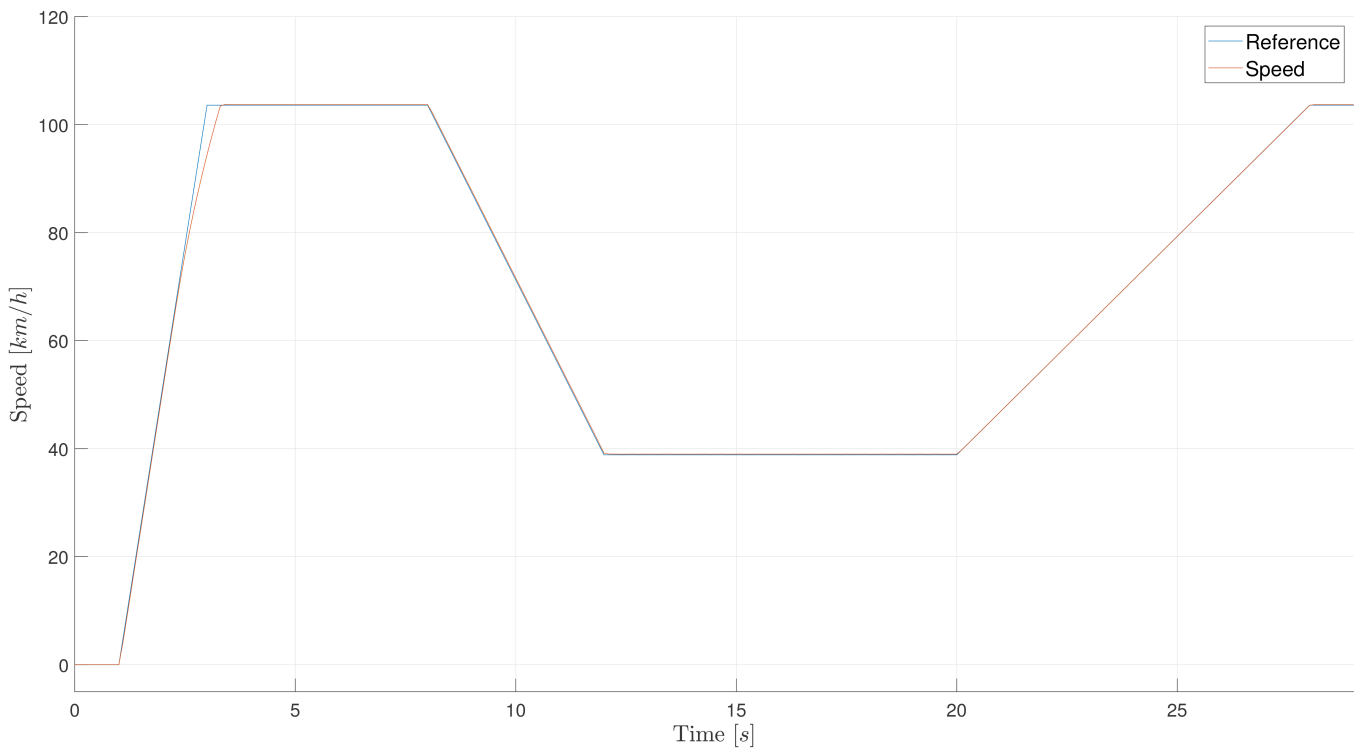
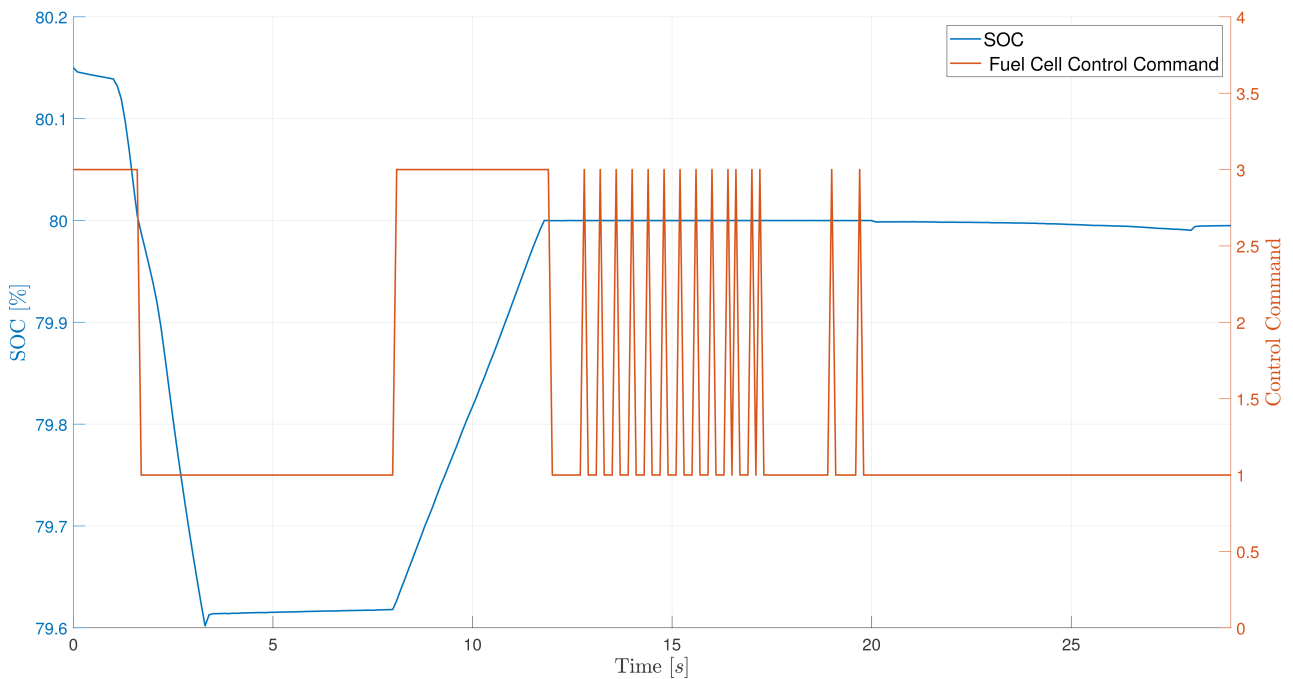


Figure 19. Control command and evolution of battery SOC with 50% SOC.



**Figure 20.** Speed performance of the FCEV with 80% of % SOC.

It is worth noting that, in the section between 10 and 18 s where, the battery is just at 80%. At this point, the algorithm starts to alternate between the two modes of operation as the battery remains at 80%. The alternation is fast enough so that, on the scale shown in the graph, changes in the SOC are indistinguishable. However, as soon as the power demand increases, the operating mode remains at 1 so that the battery provides the necessary energy and thus keeps the battery SOC stable, as seen between seconds 20 and 30.



**Figure 21.** Control command and evolution of battery SOC whitwith 80% SOC.

After observing the experiments, it can be concluded that the functioning of the control algorithm in charge of energy management works as expected. It fulfills its function of keeping the SOC between 50% and 80% while consuming as little hydrogen as possible. The most remarkable thing about this rule-based algorithm is what was seen in the last test where the SOC is close to 80%. When the power demand is allowed to settle the SOC at one of the aforementioned points, such as 80% or 50%, due to the nature of the control, the operating modes of the battery oscillate between one value and other because different functions of the algorithm are activated alternately. This could be considered non-optimal as it is constantly changing the operation of the FC and this could affect to its degradation and RUL. In order to solve this problem, a hysteresis region could be implemented in the algorithm when changing sections to cause slower oscillations and therefore less stress on the stack. Nevertheless, the aim of this work is to maintain the battery level as static as possible and, as observed in Figure 21, this task was successfully achieved. If a hysteresis region were to be implemented, the battery level would vary between the hysteresis region which will be worse for the battery. At this point, a further study to discuss the relation of the battery degradation and PEMFC degradation should be performed, which remains beyond the scope of the presented work.

Furthermore, the experiment where the ON/OFF behavior is shown, a critical point was specifically selected to show this phenomenon. However, in a real-life scenario, it is rare to exactly be at the conditions shown in the experiment where this continuous ON/OFF behavior happens.

## 5. Conclusions

Hydrogen is emerging as a proposal in the automotive industry to reduce atmospheric pollution and to try another approach to electric cars, giving another option to electric mobility. FCEVs are vehicles that use fuel cells together with a battery pack and/or a super-capacitor to power an electric induction motor.

Due to the different power sources that are used, an optimal energy consumption strategy is necessary for an efficient use of energy and hydrogen. For this task, several strategies have been studied and implemented, such as those based on optimization algorithms including ECMS or genetic algorithms and strategies based on artificial intelligence like neural networks or reinforcement learning. However, rule-based strategies have the lowest computational cost and are the most widely used in the current hydrogen car industry.

In this work, a rule-based operation mode control strategy for the EMS of a FCEV was consolidated and improved. This has been validated by means of a NEDC and WLTC driving cycle experiment and tests at different SOC operating points of the battery. In the NEDC test, the control algorithm achieves a maximum variation of 2% on a 12 kWh battery and a hydrogen consumption of 1.2 kg/100 km, while in WLTC, a consumption of 1.07 kg/100 km with a SOC variation of 1.24% is achieved.

For future developments, it would be useful to test the same algorithm but with a more complex topology by adding a super-capacitor to the DC/DC bus. This would require considering the SOC of the new element and adding it as an input to the EMS algorithm. This would obviously complicate the rules of the algorithm by having to design, modify, and add new rules.

As a further innovation, although the main task of maintaining the battery SOC is fulfilled, a function could be added to the current algorithm to smooth the changes between the different modes imposed by the EMS in order to avoid jumps between operating modes and improve fuel cell RUL as seen in the last test.

**Author Contributions:** Conceptualization, O.B. and J.U.; methodology, O.B., J.U. and E.A.; investigation, J.U. and A.d.R.; software, J.U. and E.A.; writing—original draft preparation, J.U.; writing—review and editing, J.U. and O.B.; visualization, J.U., A.d.R. and E.A.; supervision, O.B. and I.C.; project administration, O.B. and I.C. All authors have read and agreed to the published version of the manuscript.



**Funding:** The authors wish to express their gratitude to the Basque Government, through the project EKOHEGAZ II (ELKARTEK KK-2023/00051), to the Diputación Foral de Álava (DFA), through the project CONAVANTER, to the UPV/EHU, through the project GIU23/002, and to the MobilityLab Foundation (CONV23/14, CONV23/12) for supporting this work.

**Institutional Review Board Statement:** Not applicable.

**Informed Consent Statement:** Not applicable.

**Data Availability Statement:** The data presented in this study are available upon request from the corresponding author.

**Conflicts of Interest:** The authors declare no conflicts of interest.

## References

- European Environment Agency. Key Trends and Drivers in Greenhouse Gas Emissions in the EU in 2015 and the Past 25 Years. Available online: <https://www.eea.europa.eu/publications/key-trends-and-drivers-in> (accessed on 15 April 2024).
- Rivas, S.; Urraca, R.; Bertoldi, P.; Thiel, C. Towards the EU Green Deal: Local key factors to achieve ambitious 2030 climate targets. *J. Clean. Prod.* **2021**, *320*, 128878. [[CrossRef](#)]
- Aminudin, M.A.; Kamarudin, S.K.; Lim, B.H.; Majilan, E.H.; Masdar, M.S.; Shaari, N. An overview: Current progress on hydrogen fuel cell vehicles. *Int. J. Hydrog. Energy* **2023**, *48*, 4371–4388. [[CrossRef](#)]
- Mofolasayo, A. Assessing and Managing the Direct and Indirect Emissions from Electric and Fossil-Powered Vehicles. *Sustainability* **2023**, *15*, 1138. [[CrossRef](#)]
- Zou, C.; Xiong, B.; Xue, H.; Zheng, D.; Ge, Z.; Wang, Y.; Jiang, L.; Pan, S.; Wu, S. The role of new energy in carbon neutral. *Pet. Explor. Dev.* **2021**, *48*, 480–491. [[CrossRef](#)]
- Sun, C.; Zhang, H. Review of the Development of First-Generation Redox Flow Batteries: Iron-Chromium System. *ChemSusChem* **2022**, *15*, e202101798. [[CrossRef](#)] [[PubMed](#)]
- European Parliament and the Council. Regulation (EU) 2019/631 of the European Parliament and of the Council. Setting CO<sub>2</sub> Emission Performance Standards for New Passenger Cars and for New Light Commercial Vehicles, and Repealing Regulations (EC) No 443/2009 and (EU) No 510/2011. Available online: <https://eur-lex.europa.eu/legal-content/EN/TXT/?uri=CELEX%3A02019R0631-20231203> (accessed on 12 April 2024).
- Chan, C.C. The state of the art of electric, hybrid, and fuel cell vehicles. *Proc. IEEE* **2007**, *95*, 704–718. [[CrossRef](#)]
- Manoharan, Y.; Hosseini, S.E.; Butler, B.; Alzahrani, H.; Senior, B.T.F.; Ashuri, T.; Krohn, J. Hydrogen fuel cell vehicles; Current status and future prospect. *Appl. Sci.* **2019**, *9*, 2296. [[CrossRef](#)]
- Alvarez-Meaza, I.; Zarrabeitia-Bilbao, E.; Rio-Belver, R.M.; Garechana-Anacabe, G. Fuel-cell electric vehicles: Plotting a scientific and technological knowledge map. *Sustainability* **2020**, *12*, 2334. [[CrossRef](#)]
- Parikh, A.; Shah, M.; Prajapati, M. Fuelling the sustainable future: A comparative analysis between battery electrical vehicles (BEV) and fuel cell electrical vehicles (FCEV). *Environ. Sci. Pollut. Res.* **2023**, *30*, 57236–57252. [[CrossRef](#)]
- Oladosu, T.L.; Pasupuleti, J.; Kiong, T.S.; Koh, S.P.J.; Yusaf, T. Energy management strategies, control systems, and artificial intelligence-based algorithms development for hydrogen fuel cell-powered vehicles: A review. *Int. J. Hydrogen Energy* **2024**, *61*, 1380–1404. [[CrossRef](#)]
- Zhao, X.; Wang, L.; Zhou, Y.; Pan, B.; Wang, R.; Wang, L.; Yan, X. Energy management strategies for fuel cell hybrid electric vehicles: Classification, comparison, and outlook. *Energy Convers. Manag.* **2022**, *270*, 116179. [[CrossRef](#)]
- Chandra, I.; Singh, N.K.; Samuel, P. A Rule-based Energy Management Scheme for Grid-Integrated PV-Battery-powered EV Charging Station. In Proceedings of the 2022 IEEE Students Conference on Engineering and Systems, SCES 2022, Prayagraj, India, 1–3 July 2022. [[CrossRef](#)]
- Zhang, Z.; Zhang, T.; Hong, J.; Zhang, H.; Yang, J. Energy Management Optimization of Master–Slave Hybrid Electric Vehicle under Rule-Based Control Strategy. *Energy Technol.* **2022**, *10*, 2200630. [[CrossRef](#)]
- Hu, Z.; Li, J.; Xu, L.; Song, Z.; Fang, C.; Ouyang, M.; Dou, G.; Kou, G. Multi-objective energy management optimization and parameter sizing for proton exchange membrane hybrid fuel cell vehicles. *Energy Convers. Manag.* **2016**, *129*, 108–121. [[CrossRef](#)]
- Matthieu, M.; Toufik, A.; Mehdi, M.; Chaibet, A. Real-time and multi-layered energy management strategies for fuel cell electric vehicle overview. In Proceedings of the 2022 IEEE 95th Vehicular Technology Conference: (VTC2022-Spring), Helsinki, Finland, 19–22 June 2022. [[CrossRef](#)]
- Zhu, L.; Tao, F.; Fu, Z.; Wang, N.; Ji, B.; Dong, Y. Optimization Based Adaptive Cruise Control and Energy Management Strategy for Connected and Automated FCHEV. *IEEE Trans. Intell. Transp. Syst.* **2022**, *23*, 21620–21629. [[CrossRef](#)]
- Wang, T.; Li, Q.; Wang, X.; Qiu, Y.; Liu, M.; Meng, X.; Li, J.; Chen, W. An optimized energy management strategy for fuel cell hybrid power system based on maximum efficiency range identification. *J. Power Sources* **2020**, *445*, 227333. [[CrossRef](#)]
- Gao, H.; Yin, B.; Pei, Y.; Gu, H.; Xu, S.; Dong, F. An energy management strategy for fuel cell hybrid electric vehicle based on a real-time model predictive control and ponytrayin’s maximum principle. *Int. J. Green Energy* **2024**, 1–13 [[CrossRef](#)]
- Holtwerth, A.; Xhonneux, A.; Müller, D. Closed loop model predictive control of a hybrid battery-hydrogen energy storage system using mixed-integer linear programming. *Energy Convers. Manag. X* **2024**, *22*, 100561. [[CrossRef](#)]

22. Álvarez Fernández, R.; Caraballo, S.C.; Cilleruelo, F.B.; Lozano, J.A. Fuel optimization strategy for hydrogen fuel cell range extender vehicles applying genetic algorithms. *Renew. Sustain. Energy Rev.* **2018**, *81*, 655–668. [[CrossRef](#)]
23. Wieczorek, M.; Lewandowski, M. A mathematical representation of an energy management strategy for hybrid energy storage system in electric vehicle and real time optimization using a genetic algorithm. *Appl. Energy* **2017**, *192*, 222–233. [[CrossRef](#)]
24. Sorlei, I.S.; Bizon, N.; Thounthong, P.; Varlam, M.; Carcadea, E.; Culcer, M.; Iliescu, M.; Raceanu, M. Fuel Cell Electric Vehicles—A Brief Review of Current Topologies and Energy Management Strategies. *Energies* **2021**, *14*, 252. [[CrossRef](#)]
25. Majed, C.; Karaki, S.H.; Jabr, R. Neural network technique for hybrid electric vehicle optimization. In Proceedings of the 18th Mediterranean Electrotechnical Conference: Intelligent and Efficient Technologies and Services for the Citizen, MELECON 2016, Lemesos, Cyprus, 18–20 April 2016. [[CrossRef](#)]
26. Lee, H.; Cha, S.W. Energy Management Strategy of Fuel Cell Electric Vehicles Using Model-Based Reinforcement Learning with Data-Driven Model Update. *IEEE Access* **2021**, *9*, 59244–59254. [[CrossRef](#)]
27. Tie, S.F.; Tan, C.W. A review of energy sources and energy management system in electric vehicles. *Renew. Sustain. Energy Rev.* **2013**, *20*, 82–102. [[CrossRef](#)]
28. Emadi, A.; Rajashekara, K.; Williamson, S.S.; Lukic, S.M. Topological overview of hybrid electric and fuel cell vehicular power system architectures and configurations. *IEEE Trans. Veh. Technol.* **2005**, *54*, 763–770. [[CrossRef](#)]
29. Yan, Y.; Li, Q.; Chen, W.; Su, B.; Liu, J.; Ma, L. Optimal Energy Management and Control in Multimode Equivalent Energy Consumption of Fuel Cell/Supercapacitor of Hybrid Electric Tram. *IEEE Trans. Ind. Electron.* **2019**, *66*, 6065–6076. [[CrossRef](#)]
30. Paladini, V.; Donato, T.; de Risi, A.; Laforgia, D. Super-capacitors fuel-cell hybrid electric vehicle optimization and control strategy development. *Energy Convers. Manag.* **2007**, *48*, 3001–3008. [[CrossRef](#)]
31. Zhou, W.; Yang, L.; Cai, Y.; Ying, T. Dynamic programming for new energy vehicles based on their work modes Part II: Fuel cell electric vehicles. *J. Power Sources* **2018**, *407*, 92–104. [[CrossRef](#)]
32. Gurz, M.; Baltacioglu, E.; Hames, Y.; Kaya, K. The meeting of hydrogen and automotive: A review. *Int. J. Hydrog. Energy* **2017**, *42*, 23334–23346. [[CrossRef](#)]
33. Andujar Marquez, J.; Segura, F.; Vasallo, M.; Enrique, J. Sistema de control para la operación idónea de una pila de combustible. In Proceedings of the XXVI Jornadas de Automática, Alicante, España, 7–10 September 2005; pp. 411–417. [[CrossRef](#)]
34. Dimitrovar, Z.; Nader, W.B. PEM fuel cell as an auxiliary power unit for range extended hybrid electric vehicles. *Energy* **2022**, *239*. [[CrossRef](#)]
35. Saw, L.H.; Somasundaram, K.; Ye, Y.; Tay, A.A. Electro-thermal analysis of Lithium Iron Phosphate battery for electric vehicles. *J. Power Sources* **2014**, *249*, 231–238. [[CrossRef](#)]
36. Tremblay, O.; Dessaint, L.A. Experimental Validation of a Battery Dynamic Model for EV Applications. *World Electr. Veh. J.* **2009**, *3*, 289–298. [[CrossRef](#)]
37. He, Y.; Liu, X.T.; Zhang, C.B.; Chen, Z.H. A new model for State-of-Charge (SOC) estimation for high-power Li-ion batteries. *Appl. Energy* **2013**, *101*, 808–814. [[CrossRef](#)]
38. Kuntz, P.; Lonardoni, L.; Genies, S.; Raccurt, O.; Azaïs, P. Evolution of Safety Behavior of High-Power and High-Energy Commercial Li-Ion Cells after Electric Vehicle Aging. *Batteries* **2023**, *9*, 427. [[CrossRef](#)]
39. Wang, X.; Zhang, Y.; Deng, Y.; Yuan, Y.; Zhang, F.; Lv, S.; Zhu, Y.; Ni, H. Effects of Different Charging Currents and Temperatures on the Voltage Plateau Behavior of Li-Ion Batteries. *Batteries* **2023**, *9*, 42. [[CrossRef](#)]
40. Gillespie, T.D. *Fundamentals of Vehicle Dynamics*; SAE: Warrendale, PA, USA, 1992. [[CrossRef](#)]
41. Changizian, S.; Ahmadi, P.; Raeesi, M.; Javani, N. Performance optimization of hybrid hydrogen fuel cell-electric vehicles in real driving cycles. *Int. J. Hydrogen Energy* **2020**, *45*, 35180–35197. [[CrossRef](#)]
42. Hames, Y.; Kaya, K.; Baltacioglu, E.; Turksoy, A. Analysis of the control strategies for fuel saving in the hydrogen fuel cell vehicles. *Int. J. Hydrogen Energy* **2018**, *43*, 10810–10821. [[CrossRef](#)]
43. Reddy, N.P.; Padeloup, D.; Zadeh, M.K.; Skjetne, R. An Intelligent Power and Energy Management System for Fuel Cell/Battery Hybrid Electric Vehicle Using Reinforcement Learning. In Proceedings of the ITEC 2019—2019 IEEE Transportation Electrification Conference and Expo, Detroit, MI, USA, 19–21 June 2019. [[CrossRef](#)]
44. Shim, B.J.; Park, K.S.; Koo, J.M.; Jin, S.H. Work and speed based engine operation condition analysis for new European driving cycle (NEDC). *J. Mech. Sci. Technol.* **2014**, *28*, 755–761. [[CrossRef](#)]
45. Lasocki, J. The WLTC vs. NEDC: A Case Study on the Impacts of Driving Cycle on Engine Performance and Fuel Consumption. *Int. J. Automot. Mech. Eng.* **2021**, *18*, 9071–9081. [[CrossRef](#)]

**Disclaimer/Publisher’s Note:** The statements, opinions and data contained in all publications are solely those of the individual author(s) and contributor(s) and not of MDPI and/or the editor(s). MDPI and/or the editor(s) disclaim responsibility for any injury to people or property resulting from any ideas, methods, instructions or products referred to in the content.